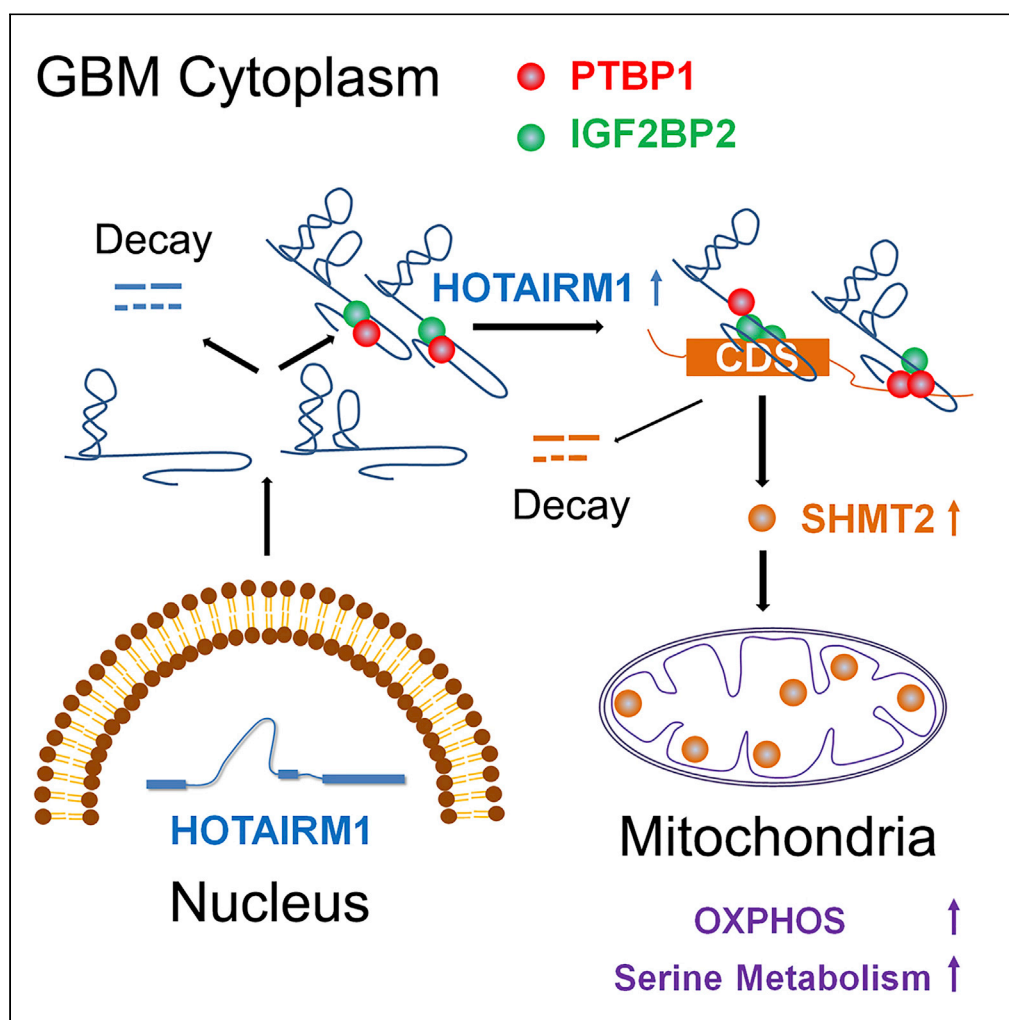


Article

Targeting HOTAIRM1 ameliorates glioblastoma by disrupting mitochondrial oxidative phosphorylation and serine metabolism



Wei Han,
Shanshan Wang,
Yingjiao Qi, Fan
Wu, Ningyu Tian,
Boqin Qiang,
Xiaozhong Peng

hanwei2012@ibms.pumc.edu.cn (W.H.)
pengxiaozhong@pumc.edu.cn (X.P.)

Highlights

HOTAIRM1 regulates mitochondrial activity in GBM

The target genes of HOTAIRM1 and the interacting RBPs were screened and identified

SHMT2 mRNA has an m⁶A site that can be recognized by IGF2BP2

HOTAIRM1 regulates the stability of *SHMT2* by binding to PTBP1 and IGF2BP2

Article

Targeting HOTAIRM1 ameliorates glioblastoma by disrupting mitochondrial oxidative phosphorylation and serine metabolism

Wei Han,^{1,*} Shanshan Wang,¹ Yingjiao Qi,¹ Fan Wu,^{1,3} Ningyu Tian,¹ Boqin Qiang,¹ and Xiaozhong Peng^{1,2,4,*}

SUMMARY

Serine hydroxymethyltransferase 2 (SHMT2), which catalyzes the conversion of serine to glycine and one-carbon transfer reactions in mitochondria, is significantly upregulated in glioblastoma (GBM). However, the mechanism by which the stability of SHMT2 gene expression is maintained to drive GBM tumorigenesis has not been clarified. Herein, through microarray screening, we identified that HOXA Transcript Antisense RNA, Myeloid-Specific 1 (HOTAIRM1) modulates the SHMT2 level in various GBM cell lines. Serine catabolism and mitochondrial oxidative phosphorylation activities were decreased by HOTAIRM1 inhibition. Mechanistically, according to our mass spectrometry and eCLIP-seq results, HOTAIRM1 can bind to PTBP1 and IGF2BP2. Furthermore, HOTAIRM1 maintains the stability of SHMT2 by promoting the recognition of an m⁶A site and the interaction of PTBP1/IGF2BP2 with SHMT2 mRNA. The stability of HOTAIRM1 can also be enhanced and results in positive feedback regulation to support the progression of GBM. Thus, targeting HOTAIRM1 could be a promising metabolic therapy for GBM.

INTRODUCTION

Glioblastoma (GBM) is considered to be a genetic disease involving multistep genomic alterations; it accounts for approximately 57% of all gliomas and is the most common and most aggressive primary malignant brain tumor in adults (Van Meir et al., 2010). Advances in next-generation sequencing technology have led to a more comprehensive understanding of the molecular profile and genomic landscape of GBM (Hu et al., 2018; Jiang et al., 2021). However, despite these advances, the prognosis of patients with GBM is still not optimistic, and the 5-year survival rate remains <10% (Tan et al., 2020). Therefore, more precise and effective molecular markers need to be found to enhance the understanding of the GBM pathogenesis and ultimately improve the outcome of patients.

The human genome contains ~20,000 protein-coding genes, accounting for less than 2% of the total genome, whereas up to 70% of the human genome is transcribed into RNAs, most of which do not have protein-coding potential (Derrien et al., 2012). Long non-coding RNAs (lncRNAs) are traditionally defined as transcripts that are longer than 200 nt and encode no identifiable proteins (Uszczynska-Ratajczak et al., 2018; Palazzo and Koonin, 2020). To date, more than 100,000 lncRNA genes have been discovered, but only a few thousand have been functionally characterized at the molecular level; these lncRNAs can modulate the structure and function of chromatin and the transcription of adjacent and distal genes, and can affect RNA splicing, stability, and translation depending on their localization and their specific interactions with DNA, RNA, and protein molecules (Li et al., 2021; Yao et al., 2019; Statello et al., 2021). Big data analysis of cancer transcriptomes has revealed thousands of lncRNAs whose aberrant expression is associated with different cancer types (Huarte, 2015). In particular, with the increasing identification of functional lncRNAs aberrantly expressed in glioma tissues and cell lines, the critical role of lncRNAs in the initiation, progression and other malignant phenotypes of glioma has attracted extensive attention (Peng et al., 2018). Consequently, exploring the precise molecular mechanisms of lncRNAs will advance their potential clinical applications as prospective novel biomarkers and therapeutic targets for glioma (Kim et al., 2021).

In 2009, Zhang et al. found that a sequence of DNA with transcriptional activity was located between the *HOXA1* and *HOXA2* genes. The novel gene did not encode proteins and was termed Hox antisense

¹State Key Laboratory of Medical Molecular Biology, Department of Molecular Biology and Biochemistry, Institute of Basic Medical Sciences, Medical Primate Research Center, Neuroscience Center, Chinese Academy of Medical Sciences, School of Basic Medicine Peking Union Medical College, Beijing 100005, China

²National Human Diseases Animal Model Resource Center, Beijing Engineering Research Center for Experimental Animal Models of Human Critical Diseases, Institute of Laboratory Animal Science, Chinese Academy of Medical Sciences & Peking Union Medical College, Beijing 100021, China

³Department of Molecular Neuropathology, Beijing Neurosurgical Institute, Capital Medical University, Beijing 100070, China

⁴Lead contact

*Correspondence: hanwei2012@ibms.pumc.edu.cn (W.H.), pengxiaozhong@pumc.edu.cn (X.P.)

<https://doi.org/10.1016/j.isci.2022.104823>



intergenic RNA myeloid 1 (HOTAIRM1) (Zhang et al., 2009). The HOTAIRM1 gene structure consists of three exons and is highly conserved in mammals (Yu et al., 2012). Its expression can be induced by retinoic acid (RA), and it was discovered to be an important regulator of myeloid cell differentiation of NB4 promyelocytic leukemia cells (Zhang et al., 2014; Wei et al., 2016; Chen et al., 2017). In addition, HOTAIRM1 has been shown to be a significant cancer-related lncRNA abnormally expressed in a variety of solid tumors such as colorectal cancer, lung cancer, and renal cell carcinoma (Wan et al., 2016; Tian et al., 2018; Hamilton et al., 2020). In gliomas, HOTAIRM1 is one of the few lncRNAs, that was found to be more highly expressed in glioma samples in multiple databases and to be upregulated in high grade gliomas (Zhang and Leung, 2014; Zhang et al., 2012). Moreover, HOTAIRM1 expression was found to be higher in recurrent gliomas than in primary gliomas (Chen et al., 2015). Unfortunately, systematic screening and exploration of the target genes of HOTAIRM1 is still lacking. Studies on the molecular mechanism of HOTAIRM1 in both GBM cells and glioma stem cells, are limited to the regulation of HOXA cluster genes (Li et al., 2018; Xia et al., 2020) and to the indirect effects on microRNA target genes via the formation of ceRNA networks (Liang et al., 2019; Wang et al., 2021). In this study, we identified two transcripts variants of HOTAIRM1 that are highly expressed in GBM. Moreover, we discovered the regulatory potential of HOTAIRM1 in mitochondrial function. More importantly, we systematically screened the functional target genes of HOTAIRM1 and verified two RNA-binding proteins interacting with HOTAIRM1. Thus, our study uncovers the previously unrecognized molecular mechanism by which HOTAIRM1 regulates mitochondrial metabolism in GBM and provides a promising new target for GBM therapy.

RESULTS

Two transcript variants of HOTAIRM1 are specifically elevated in gliomas

To further assess the potential differential expression of HOTAIRM1 in glioma samples, we used the “R2: Genomic Analysis and Visualization Platform” at <http://r2.amc.nl>. Six glioma datasets containing 681 glioma samples and one non-tumor brain tissue dataset containing 44 control samples were analyzed with MAS 5.0. HOTAIRM1 was highly expressed in the 6 glioma datasets (Figure 1A). Next, we used the GEPIA web server to analyze HOTAIRM1 expression and its relationship with prognosis in low-grade glioma (LGG) and GBM samples (Tang et al., 2017). Compared with those in normal tissues, HOTAIRM1 expression levels were significantly increased in GBM patient samples (Figure 1B). The survival rate and time of patients with high HOTAIRM1 expression were significantly decreased (Figure 1C). In 325 glioma samples from the Chinese Glioma Genome Atlas (CGGA) database, the level of HOTAIRM1 in grade III–IV gliomas was significantly higher than that in grade II gliomas (Figure 1D). Survival analysis showed results similar to those obtained with GEPIA (Figure 1E).

Next, we analyzed the expression of HOTAIRM1 in glioma cells, and found that two spliced transcripts of HOTAIRM1 were amplified simultaneously (Figure 1F). Wang et al. reported an unspliced transcript of HOTAIRM1 containing more than 4 kb and two introns in NT2-D1 cells; this transcript contributed to the physical dissociation of chromatin loops at the proximal end of the cluster (Wang et al., 2017). However, unspliced HOTAIRM1 in total RNA mixed with a small amount of genomic DNA (gDNA) was detected at a much higher level than in cDNA, which indicates that unspliced HOTAIRM1 is not the main transcript expressed in gliomas (Figure 1G). We identified the two spliced transcripts of HOTAIRM1, namely, HOTAIRM1-1 and HOTAIRM1-2 by sequencing. The full lengths of HOTAIRM1-1 and HOTAIRM1-2 were 1060 bp and 768 bp, respectively (Figure 1H). Next, we designed primers that can specifically detect HOTAIRM1-1 and HOTAIRM1-2 or simultaneously detect both variants of HOTAIRM1 in real-time PCR (qPCR) analysis (Figure 1H). We found that removal of gDNA during reverse transcription had little effect on the detection of the two HOTAIRM1 variants (Figure 1I). The expression of these two major transcript variants of HOTAIRM1 was increased in most glioma cell lines compared with normal human astrocytes (Figure 1J). To explore the localization of HOTAIRM1 in glioma cells, we selected the cytoplasmic, fully spliced transcript CRNDE (g) and the nuclear intronic transcript gVC-In4 as controls (Ellis et al., 2014). By extraction of cytoplasmic and nuclear RNAs and qPCR analysis, we found that HOTAIRM1-1 was mainly expressed in the cytoplasm, while HOTAIRM1-2 was expressed in both the cytoplasm and nucleus (Figure S1A). The FISH results also confirmed the subcellular localization of HOTAIRM1 (Figure S1B).

HOTAIRM1 regulates mitochondrial activity and promotes glioma cell growth

To investigate the role of HOTAIRM1 in glioma development, we stably transduced U87MG, T98G and A172 glioma cells simultaneously with packaged recombinant lentiviral vectors expressing shRNAs targeting both variants of HOTAIRM1 (Figure 2A). Knockdown of HOTAIRM1 significantly decreased the proliferation

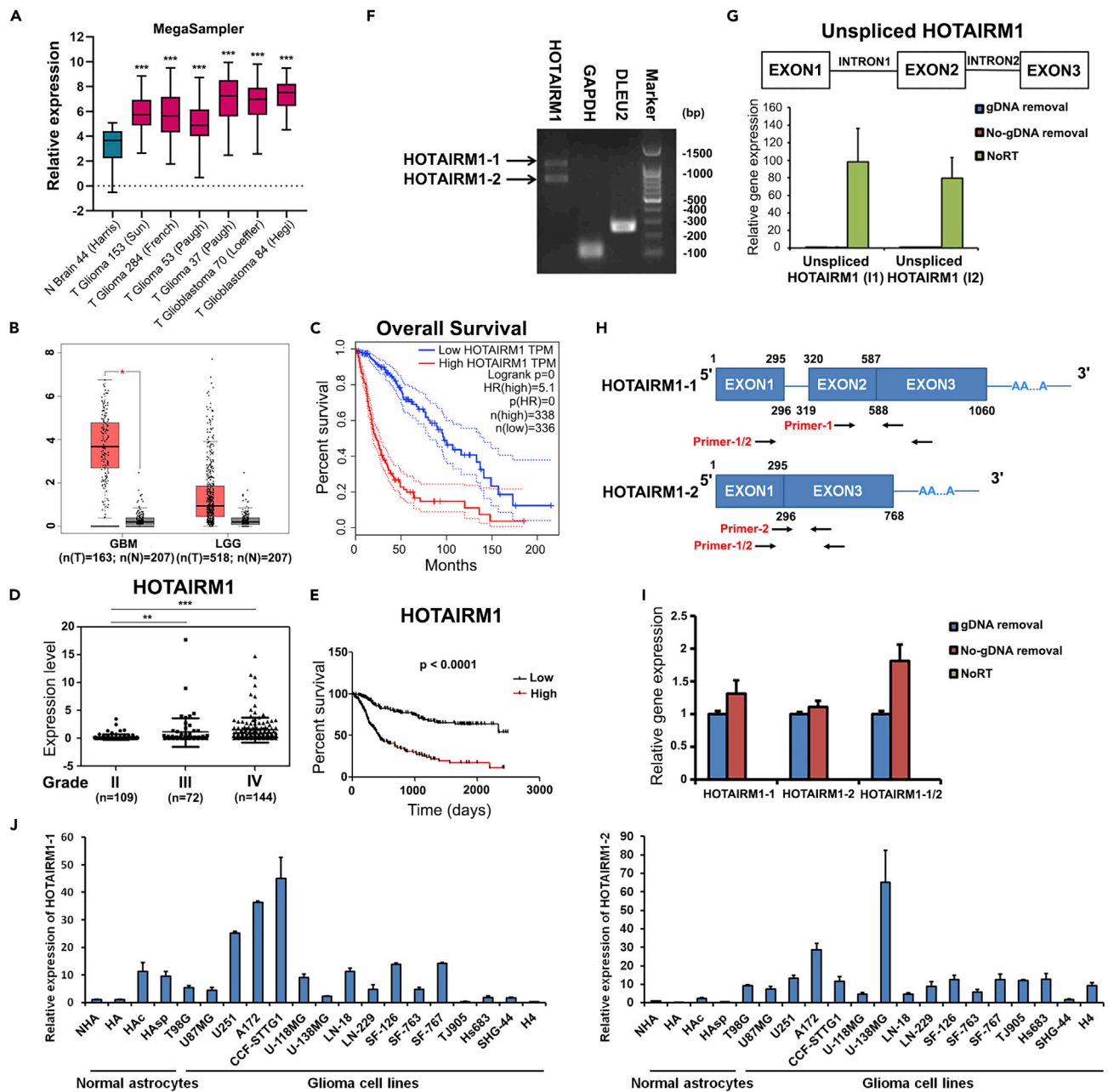


Figure 1. Two major transcript variants of HOTAIRM1 are highly expressed in glioblastomas

(A) The expression of HOTAIRM1 was analyzed using 6 glioma (T) datasets and 1 normal brain (N) dataset from R2. Data are presented as means \pm SDs (Compared with the (N) dataset, ***p < 0.001, one-way ANOVA with unpaired t test).

(B and C) Expression level and overall survival analysis of HOTAIRM1 in GBM and LGG (low-grade glioma) with the GEPIA web server. T: tumor; N: normal tissues. Data (B) are presented as means \pm SDs (*p < 0.05, unpaired t test).

(D and E) Expression level of HOTAIRM1 and overall survival analysis based on HOTAIRM1 expression in grade II–IV glioma samples from the CGGA database. Data (D) are presented as means \pm SDs (**p < 0.01, ***p < 0.001, one-way ANOVA with unpaired t test).

(F) We designed cloning primers to amplify the full length of the *HOTAIRM1* gene from A172 cell cDNA. The coding gene *GAPDH* and noncoding gene *DLEU2* were used as controls.

(G) We used two pairs of primers, I1 (INTRON 1) and I2 (INTRON 2), to detect unspliced HOTAIRM1 in the three templates (gDNA removal: cDNA with gDNA removed; no-gDNA removal: cDNA with gDNA; NoRT: only total RNA). Data are presented as means \pm SDs. (H–J) qPCR analysis of HOTAIRM1-1 and HOTAIRM1-2. GAPDH was used as the housekeeping gene. Data (I–J) are presented as means \pm SDs. See also Figure S1.

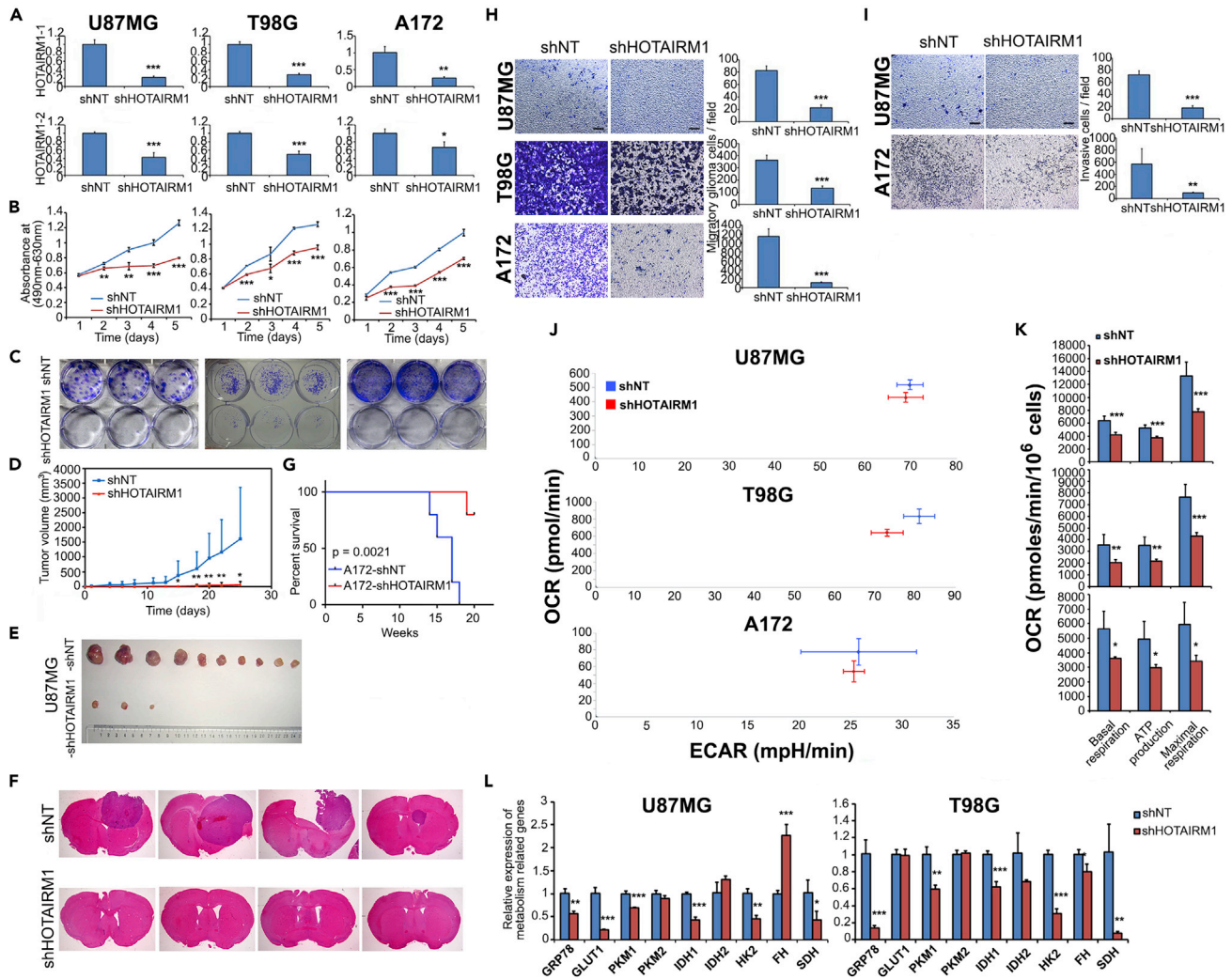


Figure 2. Inhibition of HOTAIRM1 suppresses mitochondrial function and growth of GBM cells *in vitro* and *in vivo*

(A) qPCR results showing knockdown of HOTAIRM1 in the indicated three glioma cell lines following lentiviral transduction of shHOTAIRM1. shNT served as the negative control.
 (B and C) Growth curves and colony formation assay in glioma cells with HOTAIRM1 knockdown.
 (D and E) Tumor growth curves in the U87MG cell-derived subcutaneous xenograft models (D) and tumors isolated from nude mice (E); n = 10 in each group.
 (F) The effects of HOTAIRM1 knockdown in the U87MG cell-derived intracranial xenograft mouse model (n = 4 in each group). The slices of brain tissue were stained with HE on Day 30 after implantation.
 (G) Survival statistics of tumor-bearing mice (n = 5 in each group).
 (H and I) Transwell migration (H) and invasion (I) assays of glioma cells with HOTAIRM1 knockdown were performed. Scale bar: 100 μ m.
 (J) Seahorse assays demonstrating that knockdown of HOTAIRM1 affected the oxygen consumption rate (OCR) and extracellular acidification rate (ECAR) in U87MG, T98G and A172 glioma cells.
 (K) Bar graphs showing the effect of HOTAIRM1 knockdown on basal respiration, ATP production and maximal respiration.
 (L) qPCR results showed the effect of HOTAIRM1 knockdown on the metabolism-related genes. Data (A, B, D, H, I, J, K, L) are presented as means \pm SDs (Compared with shNT, *p < 0.05, **p < 0.01, ***p < 0.001, 2-tailed Student's t test). See also Figure S1.

and colony formation of glioma cells (Figures 2B and 2C). The results of the subcutaneous and intracranial *in situ* tumorigenesis assay showed that inhibition of HOTAIRM1 expression prevented the growth of glioma cells *in vivo* and prolonged the survival of tumor bearing mice (Figures 2D–2G). We also found that the migration and invasion abilities of glioma cells were weakened by knockdown of HOTAIRM1 (Figures 2H and 2I). In particular, we found by a Seahorse assay that HOTAIRM1 can affect mitochondrial energy metabolism (Figure 2J). Compared with its effect on the extracellular acidification rate, HOTAIRM1 mainly maintained the oxygen consumption rate by regulating oxidative phosphorylation-related parameters such as

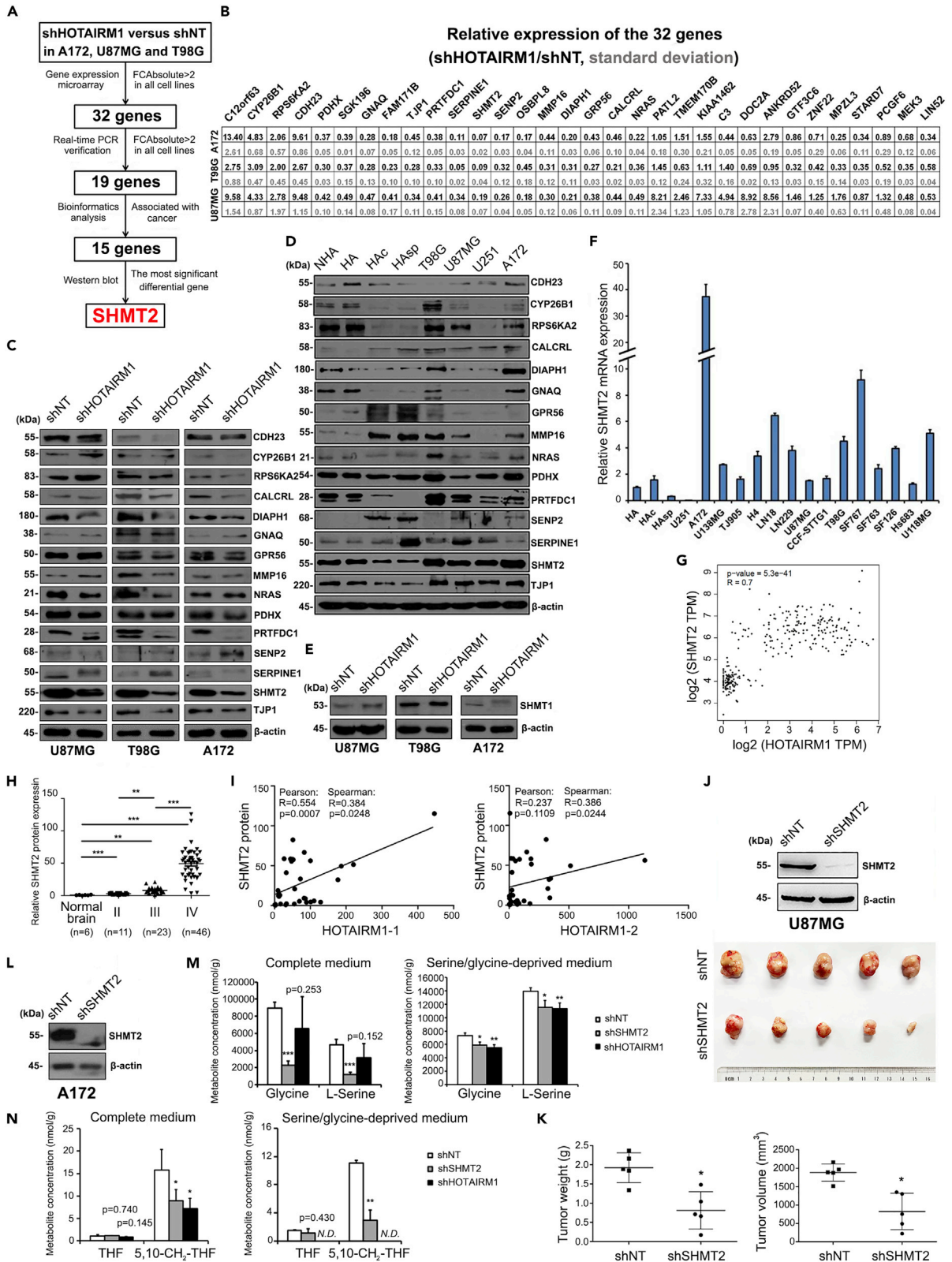


Figure 3. Screening and identification of the target genes of HOTAIRM1

- (A) Schematic outline of the process used to screen for HOTAIRM1 target genes in various GBM cell lines.
 (B) Chart showing qPCR verification of the 32 candidate target genes. Compared with shNT, data are presented as means and SDs.
 (C and D) Western blot analysis showing the changes in protein expression for the 15 candidate target genes. β -Actin was used as the loading control.
 (E) Western blot analysis showing SHMT2 protein levels.
 (F) qPCR analysis of SHMT2 in human astrocytes and glioma cell lines. Data are presented as means \pm SDs.
 (G) Spearman correlation analysis of HOTAIRM1 and SHMT2 mRNA in the brain cortex and GBM samples with the GEPIA web server.
 (H) Statistical analysis of SHMT2 protein levels in glioma tissues compared with normal brain tissues. Data are presented as means \pm SDs (**p < 0.01, ***p < 0.001, one-way ANOVA with unpaired t test).
 (I) Correlations analysis of the two HOTAIRM1 variants and the SHMT2 protein in normal brain and glioma tissues (n = 34).
 (J and K) SHMT2 knockdown xenograft tumors (shSHMT2) compared to control tumors (shNT) are pictured (J), tumor weights and volumes (K) were shown. n = 5 in each group. Data are presented as means \pm SDs (Compared with shNT, *p < 0.05, 2-tailed Student's t test).
 (L–N) After knockdown of SHMT2 (L), the glycine/L-serine (M) and THF/5,10-CH₂-THF (N) concentrations in A172 cells cultured with complete medium or serine/glycine-deprived medium were measured by UHPLC-MRM-MS. Data (M and N) are presented as means \pm SDs (Compared with shNT, *p < 0.05, **p < 0.01, ***p < 0.001, one-way ANOVA with Dunnett t test). N.D.: the target compound was not detected. See also [Figures S2, S3](#), [Tables S1](#) and [S2](#).

basal respiration, ATP production and maximal respiration ([Figure 2K](#)). We also sought to determine whether HOTAIRM1-1 and HOTAIRM1-2 can enter mitochondria ([Figures S1C](#) and [S1D](#)) using Cox III RNA transcribed from the mitochondrial genome as the control ([Kadenbach and Hüttemann, 2015](#)). Although knockdown of HOTAIRM1 did not inhibit the expression of the mitochondrial transcription factors PGC1 α ([LeBleu et al., 2014](#)) and MTF1 ([LaGory et al., 2015](#)) ([Figures S1E](#) and [S1F](#)), it did inhibit the expression of many genes related to cell metabolism ([Figure 2L](#)).

SHMT2 was identified as an important target gene of HOTAIRM1 in glioma

To screen and identify the downstream target genes of HOTAIRM1 in glioma cells, we performed a microarray analysis in U87MG, T98G and A172 cells with stable knockdown of HOTAIRM1 and initially screened 32 candidate genes with significant expression differences ([Figure 3A](#)). Subsequently, we verified the 32 candidate genes by qPCR ([Figure 3B](#)) and further screened 15 potential target genes related to cancer through bioinformatics analysis ([Table S1](#)). Then, we analyzed the effects of HOTAIRM1 knockdown on the protein levels of these 15 genes and the expression profiles of these genes in normal astrocytes lines (NHA, HA, HAc and HAsp) and glioma cell lines (T98G, U87MG, U251 and A172) by western blotting. The results showed that SHMT2 protein expression was inhibited by knockdown of HOTAIRM1, and was higher in glioma cell lines ([Figures 3C](#) and [3D](#)). SHMT2 encodes mitochondrial serine hydroxymethyltransferase (SHMT2), and catalyzes the transfer of the beta carbon of serine to tetrahydrofolate (THF) to form glycine and 5,10-CH₂-THF ([Hebbring et al., 2012](#)). Notably, knockdown of HOTAIRM1 did not affect the protein level of the cytoplasmic isozyme SHMT1 ([Figure 3E](#)). After expanding the panel of glioma cell lines, we detected the expression profile of SHMT2 by qPCR and found that the RNA level of SHMT2 was generally increased in these glioma cell lines, with the highest level in A172 cells ([Figure 3F](#)). There was a significant positive correlation between HOTAIRM1 and SHMT2 gene expression in brain cortex and GBM samples from the GEPIA web server ([Figure 3G](#)). We also evaluated the results of western blot analysis of SHMT2 in tissues, and found that the SHMT2 protein level in glioma tissues of different grades was significantly higher than that in normal brain tissues and gradually increased from grade II samples to grade IV samples ([Figure 3H](#)). SHMT2 is a potential biomarker for the diagnosis and prognosis of glioma and can drive the malignant glioma tumorigenesis ([Kim et al., 2015](#); [Wang et al., 2017](#)). There was a positive correlation between SHMT2 protein and HOTAIRM1 transcript variant expression ([Figure 3I](#)). We also performed a xenograft tumor formation assay in nude mice. On the 40th day after cell injection, we observed a statistically significant reduction in both tumor weights and volumes of knockdown SHMT2 ([Figures 3J](#) and [3K](#)). Mitochondrial one-carbon metabolism produces one-carbon unites from serine through the activity of SHMT2 ([Zhao et al., 2021](#)). Serine metabolism is an important regulator of cellular redox homeostasis and GBM cell survival ([Engel et al., 2020](#); [Tiware et al., 2020](#)). We found that similar to knockdown of SHMT2, knockdown of HOTAIRM1 reduced the contents of glycine and serine, especially after cells were treated with glycine/serine-deprived medium ([Figures 3L](#), [3M](#), and [Table S2](#)). THF and 5,10-CH₂-THF were almost undetectable in HOTAIRM1 knockdown cells treated with glycine/serine deprived medium ([Figure 3N](#)). In conclusion, we identified SHMT2 as a key target gene of HOTAIRM1 in gliomas.

HOTAIRM1 regulates the expression of SHMT2 at the posttranscriptional level

To analyze the effect of the two different variants of HOTAIRM1 on SHMT2 expression, we designed five siRNAs targeting HOTAIRM1-1 (si-1, si-2), HOTAIRM1-2 (si-3, si-4) and HOTAIRM1-1/2 (si-5) ([Figure S2A](#)),

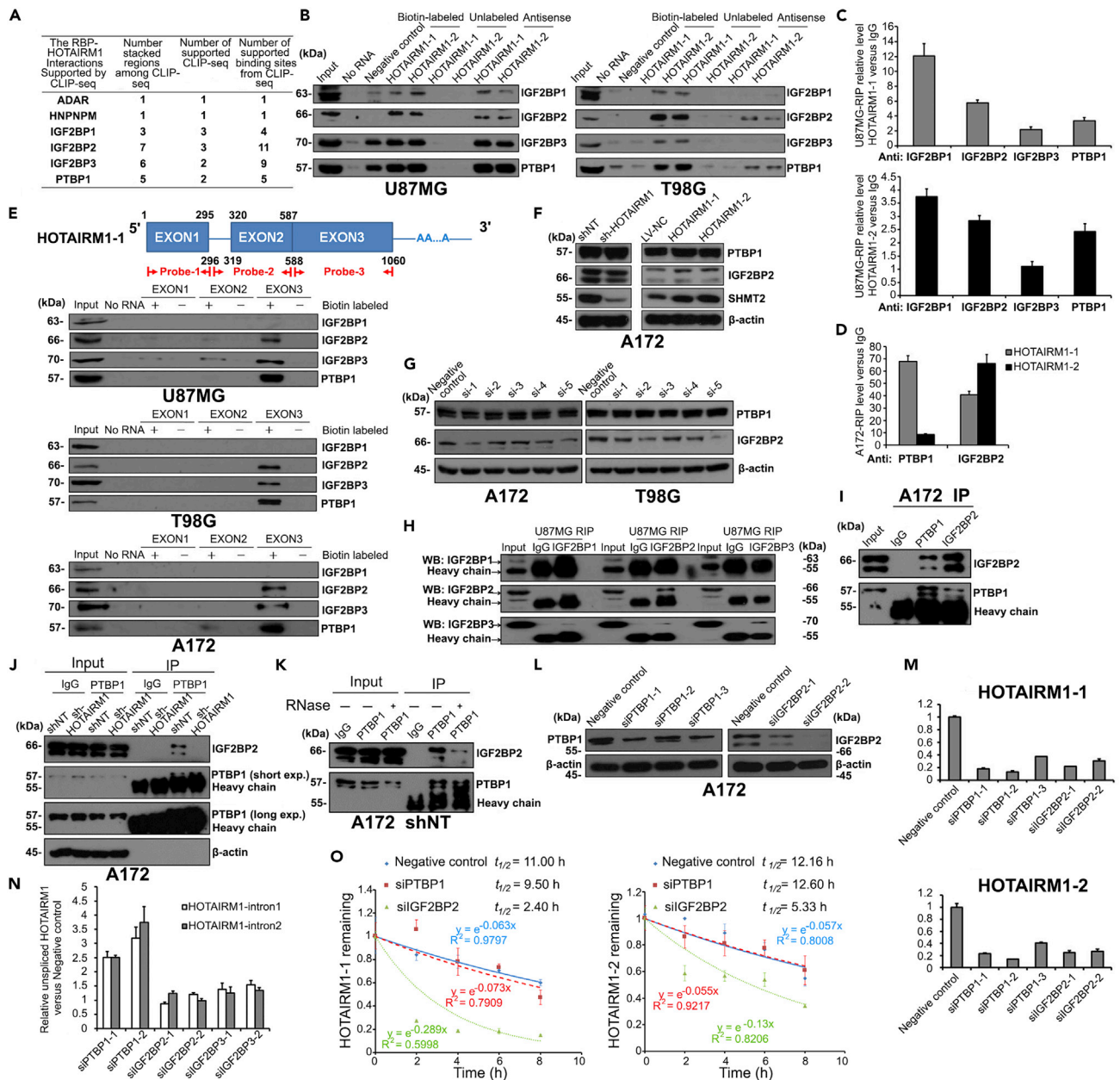


Figure 4. The HOTAIRM1-interacting proteins IGF2BP2 and PTBP1 regulate HOTAIRM1 expression

(A) Prediction of RBP targets of HOTAIRM1 binding with starBase v2.0.

(B) Biotin pull-down assay of complexes formed *in vitro* using biotin-labeled full-length sequences of the two HOTAIRM1 variants and whole-cell lysates. The indicated proteins were detected by western blotting.

(C and D) RIP-qPCR validation of HOTAIRM1 enrichment by RBPs compared to rabbit IgG in glioma cells. Data are presented as means \pm SDs.

(E) A biotin pull-down assay was used to determine which exons of HOTAIRM1 bind to IGF2BPs or the PTBP1 protein.

(F and G) Western blot analysis showing the levels of PTBP1 and IGF2BP2 in glioma cells with HOTAIRM1 knockdown or overexpression.

(H) Protein complexes were enriched by RIP, and IGF2BP proteins were detected separately by western blotting.

(I) For co-immunoprecipitation, cellular proteins were immunoprecipitated using an anti-PTBP1 or anti-IGF2BP2 antibody. The precipitates were immunoblotted with the indicated antibodies.

(J) Proteins in A172-shNT and A172-shHOTAIRM1 cells were immunoprecipitated with an anti-PTBP1 antibody. The precipitates were immunoblotted with the indicated antibodies.

(K) RNase pretreatment was performed on A172-shNT cells. Other immunoprecipitation steps were performed as described above.

Figure 4. Continued

(L–N) The effect of PTBP1 or IGF2BP2 knockdown (L) on the expression of spliced HOTAIRM1 (M) and unspliced HOTAIRM1 (N), as assessed by qPCR. Data (M and N) are presented as means \pm SDs.

(O) A BRIC assay was performed to estimate the decay rate of HOTAIRM1 by quantifying BrU-labeled RNAs after knockdown of PTBP1 or IGF2BP2. The amount of HOTAIRM1-1 or HOTAIRM1-2 remaining at each time point was determined by qPCR, and the half-life ($t_{1/2}$) was calculated. Data are presented as means \pm SDs. See also [Figures S4, S5](#) and [Table S3](#).

and all siRNAs inhibited the expression of SHMT2 and decreased the viability of glioma cells ([Figures S2B–S2E](#)). We also found that overexpression of any HOTAIRM1 transcript increased the level of SHMT2 ([Figure S2F](#)). Inhibition of HOTAIRM1-1 significantly attenuated the upregulation of SHMT2 induced by overexpression of HOTAIRM1-2, indicating that HOTAIRM1-1 had a stronger regulatory effect than HOTAIRM1-2 on SHMT2 ([Figure S2G](#)).

Next, we investigated whether HOTAIRM1 promotes the transcriptional activity of the SHMT2 promoter. However, we did not see an effect of HOTAIRM1 on SHMT2 transcriptional activity ([Figure S3A](#)). We also examined the transcription factors upstream of *SHMT2*: C-Myc, N-Myc, and HIF-1 α ([Ye et al., 2014](#)). The binding of HOTAIRM1 to the three transcription factors was weak, and knockdown of HOTAIRM1 did not change the expression of these transcription factors ([Figures S3B and S3C](#)). Induction of HIF-1 α expression by deferoxamine (DFO) did not significantly increase SHMT2 expression ([Figures S3D and S3E](#)). Based on the above results, we hypothesized that HOTAIRM1 is very likely to regulate the expression of SHMT2 at the posttranscriptional level.

Functional interaction of PTBP1 and IGF2BP2 proteins with HOTAIRM1

RNA-binding proteins (RBPs) can bind to mRNAs and noncoding RNAs and are critical to maintaining the transcriptome by post-transcriptionally controlling the expression of genes involved in cancer progression ([Qin et al., 2020](#)). Because HOTAIRM1 is also highly expressed in the cytoplasm ([Figures S1A and S1B](#)), we speculated that HOTAIRM1 may be prone to interact with RBPs, and then regulate SHMT2. A total of 22 RBPs (score >700, empAI >1) were screened by biotin pulldown followed by silver staining and mass spectrometry ([Table S3](#)). Based on the starBase v2.0 tool ([Li et al., 2014](#)), we continued to search for RBP-HOTAIRM1 interactions supported by CLIP-seq data with medium or strong stringency. Only the IGF2BPs and the PTBP1 protein were found to bind to HOTAIRM1 in more than two experiments ([Figure 4A](#)). By using biotin pulldown followed by RIP-qPCR, we verified that the IGF2BPs and PTBP1 protein interact with HOTAIRM1 in glioma cells ([Figures 4B–4D](#)). The results of biotin pulldown of HOTAIRM1 fragments showed that IGF2BP2 and PTBP1 had a greater ability to bind to HOTAIRM1 than did IGF2BP1 and IGF2BP3 when the input sample was used as the control ([Figure 4E](#)). However, the effect of HOTAIRM1 on PTBP1 and IGF2BP2 protein levels was not obvious ([Figures 4F and 4G](#)). Surprisingly, we found by RIP that the three proteins in the IGF2BP family did not interact with each other in the complex ([Figure 4H](#)); however, there was an interaction between IGF2BP2 and PTBP1 ([Figure 4I](#)), and this interaction was weakened with decreasing HOTAIRM1 expression ([Figure 4J](#)). To confirm that the interaction is dependent on a long noncoding RNA, we treated the protein complex with RNase and continued the IP experiment. The results showed that the interaction was significantly abated when RNA molecules were digested and degraded ([Figure 4K](#)).

PTBP1 and IGF2BP proteins have been reported to be involved in the growth of glioma ([Cheung et al., 2009](#); [Wang et al., 2015](#); [Janiszewska et al., 2012](#); [Suvasini et al., 2011](#)). Knockdown of these proteins, except for IGF2BP1, inhibited the proliferative activity of glioma cells as well as HOTAIRM1 expression ([Figures S4A and S4B](#)). Knockdown of either PTBP1 or IGF2BP2 effectively inhibited the expression of both variants of HOTAIRM1 ([Figures 4L and 4M](#)). Mechanistically, we detected the unspliced form of HOTAIRM1 by real-time PCR and used the 5'-bromouridine IP chase (BRIC) method ([Yamada et al., 2018](#)) to analyze the stability of HOTAIRM1. The results suggested that PTBP1 inhibited the production of unspliced HOTAIRM1 ([Figure 4N](#)), while IGF2BP2 maintained HOTAIRM1 RNA stability mainly by increasing the half-life of HOTAIRM1. Knockdown of IGF2BP2 reduced the half-lives of HOTAIRM1-1 and HOTAIRM1-2 from 11.00 to 12.16 h–2.40 and 5.33 h, respectively ([Figure 4O](#)).

PTBP1 and IGF2BP2 proteins associated and control SHMT2 mRNA

The binding sites in IGF2BP proteins contain a conserved core sequence (5'-CGGAC-3') and a variable sequence (5'-C/A-CA-C/U-3'), which can be spaced 10–30 nt apart ([Patel et al., 2012](#)). Based on this feature, we analyzed the 15 candidate target genes regulated by HOTAIRM1 and found that nine genes, including

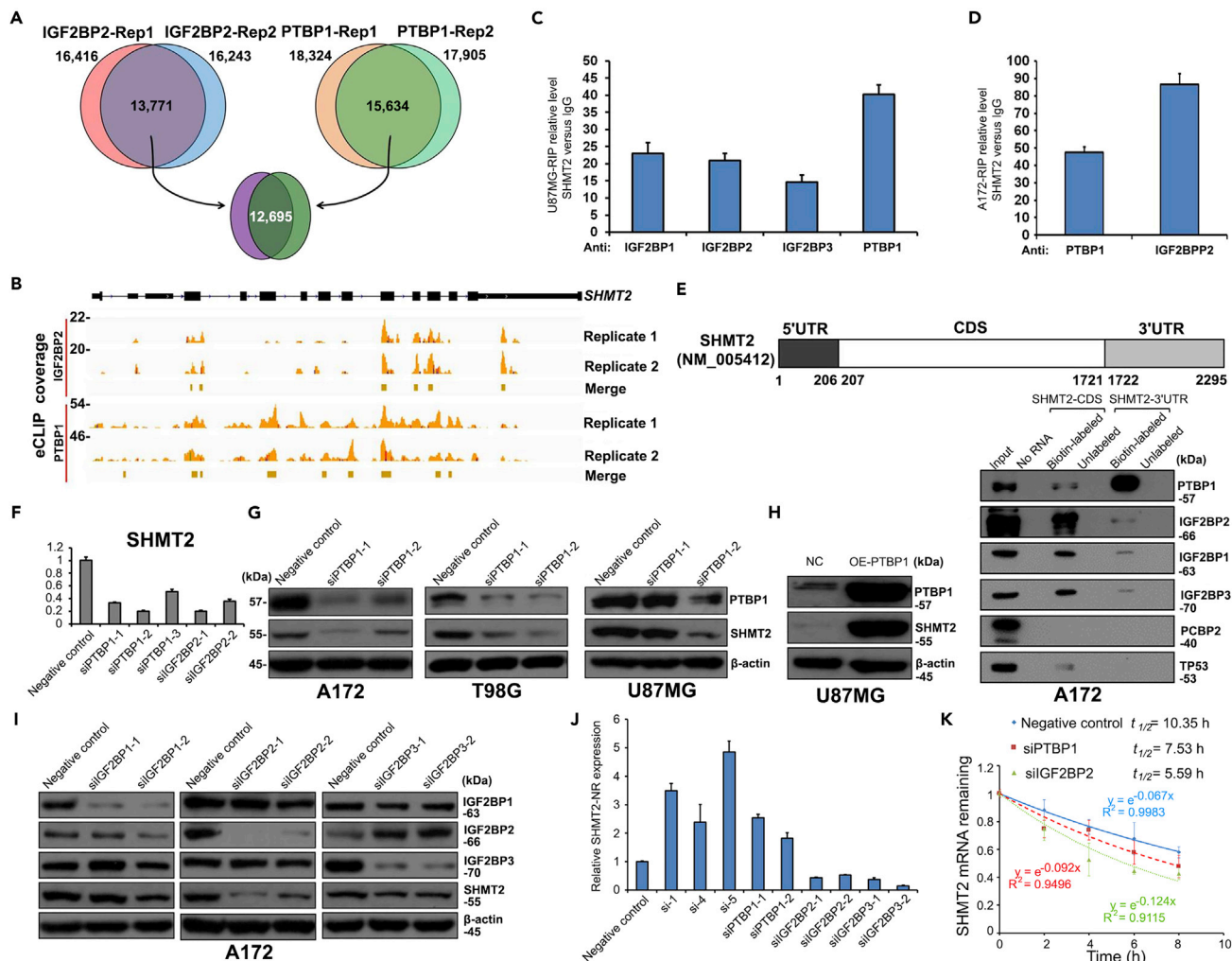


Figure 5. PTBP1 and IGF2BP2 bind to SHMT2 and regulate its expression

(A) Venn diagram comparison of peaks identified by PTBP1 and IGF2BP2 eCLIP-seq.

(B) Genome browser views of eCLIP-seq signals at SHMT2 loci.

(C and D) RIP-qPCR validation of SHMT2 mRNA enrichment. Data are presented as means \pm SDs.

(E) A biotin pulldown assay was used to determine which segment of SHMT2 mRNA binds to the RBPs.

(F–J) qPCR and western blot analyses showing the effect of PTBP1 or IGF2BP knockdown on SHMT2 expression. Data (J) are presented as means \pm SDs.

(K) A BRIC assay was performed to estimate the decay rate of SHMT2 mRNA after knockdown of PTBP1 or IGF2BP2, and $t_{1/2}$ was calculated. Data are presented as means \pm SDs. See also Table S4.

SHMT2, had binding sites for IGF2BP proteins (Table S4). To define the molecular effectors of PTBP1 and IGF2BP2, we next carried out an unbiased analysis of transcripts bound by PTBP1 and IGF2BP2 using enhanced crosslinking immunoprecipitation followed by high-throughput sequencing (eCLIP-seq) in A172 glioma cells. As previously reported (Van Nostrand et al., 2016), we repeated the eCLIP method twice in each experiment and found very high ratios of overlapping PTBP1- and IGF2BP2-binding mRNAs, with a total of 12,695 overlapping RNAs (Figure 5A). We noted both HOTAIRM1 and SHMT2 among these overlapping binding RNAs (Figures 5B and 5C). The sequence bias of enriched motifs in each eCLIP experiment is shown in Figure S4D. We verified by RIP-qPCR that both IGF2BP2 and PTBP1 enriched SHMT2 mRNA in different glioma cells (Figures 5C and 5D). Via biotin pulldown of SHMT2 fragments, we discovered that IGF2BPs mainly bind to the coding sequence (CDS) of SHMT2, while PTBP1 can bind to both the CDS and the 3' untranslated region (3'UTR) (Figure 5E). More experimental data showed that PTBP1 and IGF2BP2 but not IGF2BP1 and IGF2BP3 can modulate the mRNA and protein expression of SHMT2 (Figures 5F–5I). Some noncoding RNA (SHMT2-NR) variants that contain an alternate 5' exon and

lack an internal exon, leading to nonsense-mediated mRNA decay (NMD), can be produced from the *SHMT2* gene. Inhibition of HOTAIRM1 or PTBP1 by siRNAs increased the *SHMT2-NR* level, but inhibition of IGF2BPs did not (Figure 5J). mRNA half-life analysis based on the BRIC experiment showed that knockdown of IGF2BP2 had a greater effect on the stability of *SHMT2* mRNA than did knockdown of PTBP1, reducing the half-life from 10.35 h to 5.59 h (Figure 5K). Thus, in summary, PTBP1 and IGF2BP2 can bind to HOTAIRM1 and *SHMT2* mRNA simultaneously, and maintain the expression of *SHMT2* by inhibiting NMD and regulating *SHMT2* mRNA stability.

HOTAIRM1 is required for PTBP1 and IGF2BP2 to act on SHMT2

We used the BRIC method to detect the effect of HOTAIRM1 on the RNA half-life. The results showed that the half-life of *SHMT2* mRNA was reduced from 10.83 h to 4.15 h in cells with stable HOTAIRM1 knockdown. In the same cells, the half-lives of *PTBP1* and *IGF2BP2* mRNA did not decrease (Figures 6A–6C). RIP-qPCR showed that PTBP1 and IGF2BP2 significantly abated *SHMT2* mRNA accumulation in HOTAIRM1 knockdown cells (Figure 6D). Knockdown of HOTAIRM1 attenuated the binding of IGF2BP2 to the *SHMT2* CDS and PTBP1 to the *SHMT2* 3'UTR (Figure 6E). These results imply that the binding of PTBP1 and IGF2BP2 to *SHMT2* mRNA requires the involvement of HOTAIRM1.

Next, we focused on the mechanism by which HOTAIRM1 and IGF2BP2 enhance the stability of *SHMT2* mRNA. N⁶-methyladenosine (m⁶A) modification of mRNAs maintains mRNA stability and its dysregulation contributes to tumorigenesis (Cheng et al., 2021). IGF2BPs, as m⁶A readers, can promote the stability and accumulation of their target mRNAs (Huang et al., 2018). To determine whether *SHMT2* is subject to RNA methylation such that the methylated *SHMT2* mRNA is recognized by HOTAIRM1 and IGF2BP2, we performed RIP assays with an anti-m⁶A antibody, and five pairs of qPCR primers (to amplify exon 2, exon 8, exon 9, exon 10, and the 3'UTR) were designed based on the IGF2BP2-*SHMT2* binding peaks in two eCLIP replicates (Figure 6F). Exon 2, exon 8 and exon 9 of *SHMT2* were more enriched by the anti-m⁶A antibody, and knockdown of HOTAIRM1 reduced the ratio of meRIP enrichment to input. These results indicate that m⁶A modification of these sites depends on the expression of HOTAIRM1 (Figure 6G). Compared with the negative control, exon 2, exon 8, exon 9 and the 3'UTR of *SHMT2* were significantly enriched in glioma cells regardless of whether HOTAIRM1 was knocked down (Figure 6H). In accordance with our previous results, knockdown of HOTAIRM1 inhibited the expression of *SHMT2*, as determined by using the primers to amplify these five fragments (Figure 6I). We analyzed the sequences of exon 2, exon 8 and exon 9 in the CDS of *SHMT2*. Both exon 2 and exon 8 contained IGF2BP2 binding sites and m⁶A recognition sites (Figure 6J). These results confirmed the existence of m⁶A modification sites in *SHMT2* mRNA, and suggested that IGF2BP2 could bind to these m⁶A sites when interacting with HOTAIRM1.

HOTAIRM1 promotes glioma growth by regulating SHMT2

To verify whether the effect of HOTAIRM1 on glioma cells is caused by the change in *SHMT2* expression, we designed a rescue experiment. First, we overexpressed *SHMT2* in three glioma cell lines, and the results showed that *SHMT2* was more effective in promoting tumor growth in T98G and A172 cells (Figures 7A and 7B). Although *SHMT2* had little effect on the growth of U87MG cells *in vitro*, knockdown of *SHMT2* could still inhibit the long-term growth of U87MG cells *in vivo* (Figure 3J). Then, to eliminate the possibility of off-target effects of the shRNA, we designed an additional shRNA target. Both lentiviral shRNAs effectively inhibited the expression of both transcript variants of HOTAIRM1 and its target gene *SHMT2*, and both shRNAs also significantly attenuated the growth of glioma cells (Figures 7C–7F). Finally, we overexpressed *SHMT2* in glioma cells with stable knockdown of HOTAIRM1 and proved that *SHMT2* could rescue the growth inhibition of glioma cells with knockdown of HOTAIRM1 (Figures 7G and 7H). Evidence from Seahorse assays indicates that *SHMT2* is essential for sustaining oxidative phosphorylation (Morscher et al., 2018). We also examined the effects of PTBP1 and IGF2BP2 on mitochondrial oxidative phosphorylation. Loss of PTBP1 or IGF2BP2 reduced basal respiration, the maximal respiratory capacity and ATP production (Figures 7I and 7J). In conclusion, collectively, our data reveal the molecular mechanism by which HOTAIRM1 regulates its target gene *SHMT2* to affect GBM progression by altering mitochondrial metabolic activity.

DISCUSSION

Mitochondrial oxidative phosphorylation plays a key role in the immortalization of tumor cells, and most brain tumor cells produce energy via oxidative phosphorylation rather than glycolysis (Bonnay et al.,

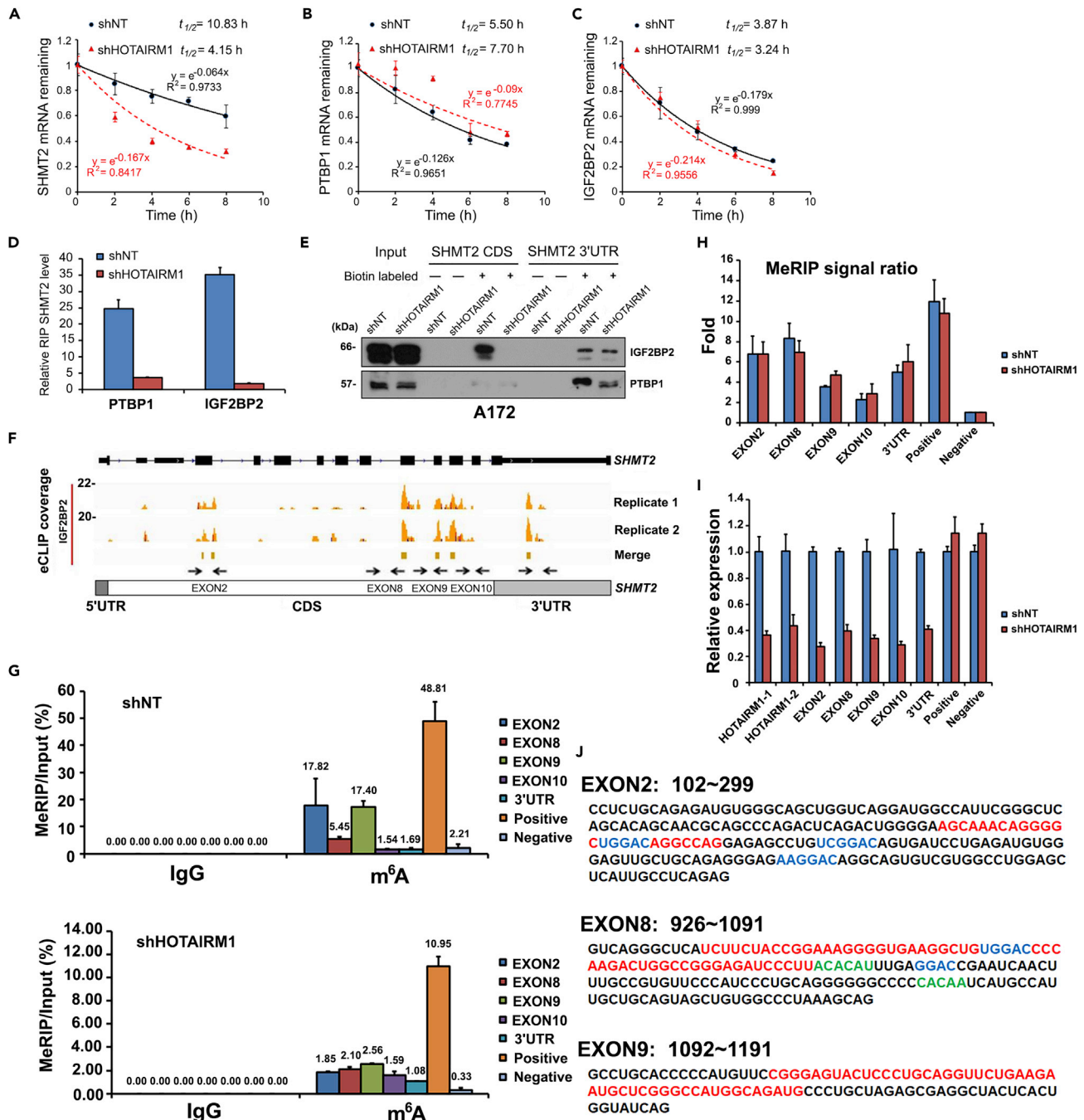


Figure 6. HOTAIRM1 regulates the stability of SHMT2 mRNA by binding PTBP1 and IGF2BP2

(A–C) A BRIC assay was performed to estimate the decay rates of SHMT2 (A), PTBP1 (B) and IGF2BP2 (C) mRNA in cells with HOTAIRM1 knockdown. Data are presented as means \pm SDs.

(D and E) Analysis of the effect of HOTAIRM1 knockdown on SHMT2 enrichment by RIP-qPCR and a biotin pull-down assay. Data (D) are presented as means \pm SDs.

(F–H) The percentages of m⁶A-enriched regions in SHMT2 compared to input RNA (G) and the m⁶A enrichment ratios relative to the negative control (H) were determined by MeRIP-qPCR. EEF1A1-positive and EEF1A1-negative region were used as controls. Data (G and H) are presented as means \pm SDs.

(I) qPCR analysis of the indicated regions in A172-shNT and A172-shHOTAIRM1 cells. Data are presented as means \pm SDs.

(J) The nucleotide sequences of exon 2, exon 8 and exon 9 in SHMT2 mRNA are displayed. Red: the IGF2BP2 binding site identified by eCLIP. Blue: the m⁶A recognition site in IGF2BP2 (Huang et al., 2018); Green: the core binding site in IGF2BP2 (Conway et al., 2016).

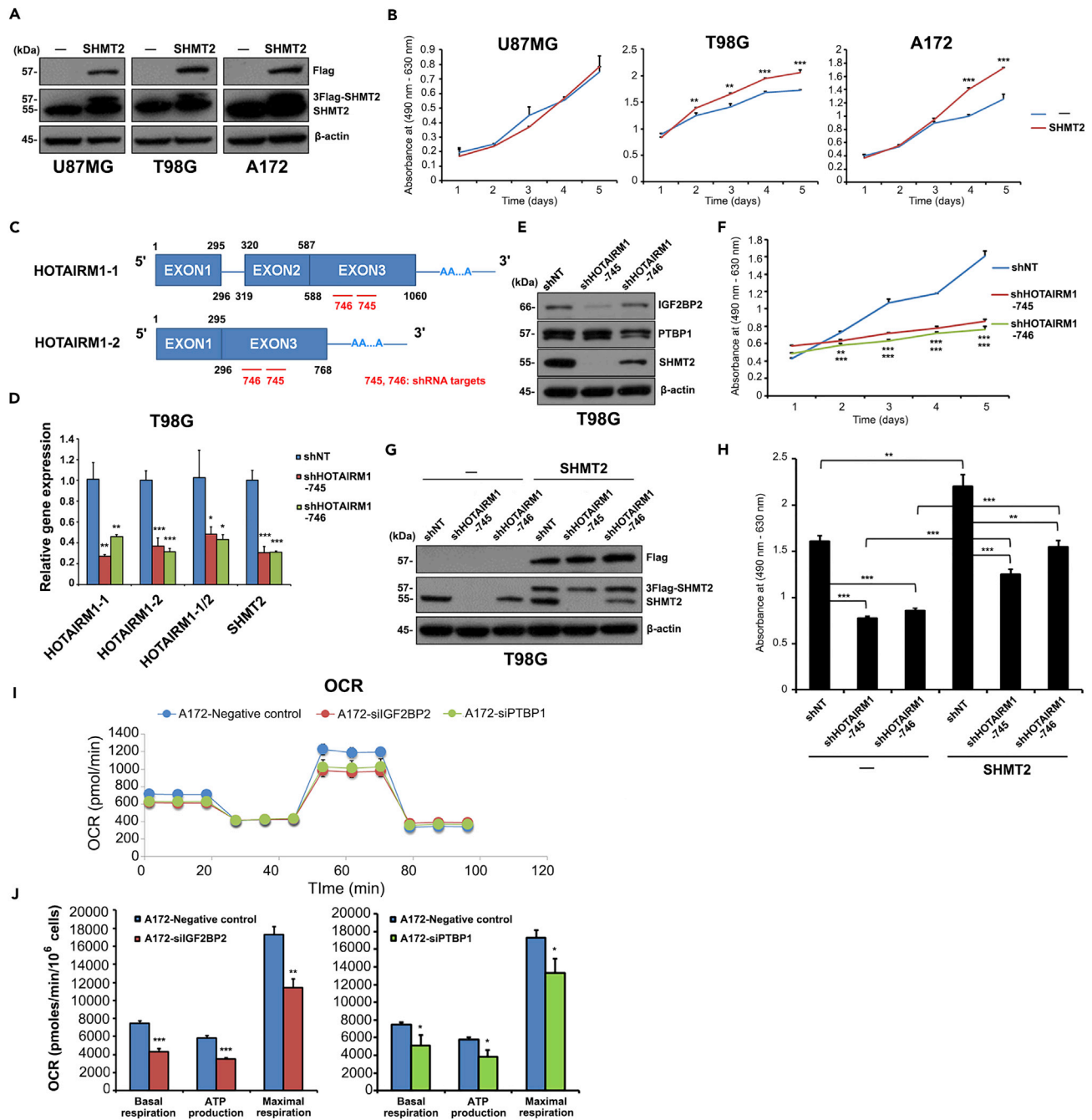


Figure 7. HOTAIRM1 regulates glioma cell activity by binding to PTBP1 and IGF2BP2 to maintain SHMT2 expression

(A) Western blot analysis of SHMT2 overexpression.

(B) Growth curves of glioma cells with SHMT2 overexpression. Data are presented as means \pm SDs (Compared with the control (–), ** $p < 0.01$, *** $p < 0.001$, 2-tailed Student’s t test).

(C–F) Analysis of the effects of lentiviral shRNA (745 and 746)-mediated HOTAIRM1 knockdown on target gene expression and cell growth. Data (D and F) are presented as means \pm SDs (Compared with shNT, * $p < 0.05$, ** $p < 0.01$, *** $p < 0.001$, one-way ANOVA with Dunnett t test).

(G and H) Western blot analysis (G) showing SHMT2 overexpression in cells with HOTAIRM1 knockdown. Bar graphs (H) showing the results of MTS assays performed 96 h after expression rescue. Data (H) are presented as means \pm SDs (** $p < 0.01$, *** $p < 0.001$, one-way ANOVA with Tukey’s test).

(I and J) Seahorse assays (I) showing the affected OCR in A172 cells with IGF2BP2 or PTBP1 knockdown. Bar graphs (J) showing the effects on basal respiration, ATP production and maximal respiration. Data (I and J) are presented as means \pm SDs (Compared with negative control, * $p < 0.05$, ** $p < 0.01$, *** $p < 0.001$, 2-tailed Student’s t test).

2020). Selective inhibition of oxidative phosphorylation in tumor cells can effectively inhibit tumor growth and metastasis by abolishing mitochondrial function (Cheng et al., 2019). Mitochondrial dynamics are tightly coordinated in association with GBM biology, leading to mitochondrial fusion and fission to alter the balance of oxidative phosphorylation, eliminate damaged mitochondrial components and regulate reactive oxygen species (Xie et al., 2015). Serine catabolism mediated by SHMT2 is necessary to maintain mitochondrial respiration and aerobic ATP production in mammalian cells (Lucas et al., 2018; Yang et al., 2020). Cancer cells also have the metabolic characteristic of serine addiction (Pacold et al., 2016; Frezza, 2016). Limiting the uptake of serine by cancer cells can induce cells to produce toxic metabolites and effectively delay the growth of tumors (Muthusamy et al., 2020). In our study, we mainly showed that HOTAIRM1 is involved in the regulation of mitochondrial function in GBM, especially oxidative phosphorylation and serine metabolism. In terms of the molecular mechanism, HOTAIRM1 can strengthen the interaction between PTBP1 and IGF2BP2, recruit them to bind to *SHMT2* mRNA, and in turn lead to an increase in the protein level of SHMT2 by enhancing the stability of its mRNA, resulting in the induction of mitochondrial activity and the malignant progression of glioma.

In more cell lines, HOTAIRM1 has also been observed to promote GBM aggressiveness. Moreover, radiosensitivity and reactive oxygen species levels, the hallmark of mitochondrial dysfunction, increase with HOTAIRM1 knockdown in GBM cells (Ahmadov et al., 2021). Previous publications reported that SHMT2 deficiency leads to mitochondrial respiration defects (Jin et al., 2022) and the accumulation of intracellular reactive oxygen species (Zhang et al., 2022). A tight connection between the mitochondrial enzyme SHMT2 and mitochondrial energy metabolism has been established. Therefore, we identified SHMT2 as an extremely crucial target of HOTAIRM1 to affect mitochondrial function. We also found that knockdown of HOTAIRM1 did not affect the expression of PHGDH and SHMT1, which suggests that HOTAIRM1 is mainly involved in serine catabolism and one-carbon unit synthesis in mitochondria. It has been shown that both desuccinylation and deacetylation of SHMT2 can drive carcinogenesis through maintaining its high enzymatic activity (Yang et al., 2018; Wei et al., 2018); STAT3 and Myc/HIF-1 α can bind to the promoter region of *SHMT2* to induce its transcription (Marrocco et al., 2019; Nikiforov et al., 2002; Haggerty et al., 2003; Ye et al., 2014); SHMT1 and miR-642a-5p participate in post-transcriptional regulation of SHMT2 by binding to the 5'UTR and -3'UTR, respectively, of the SHMT2 transcript (Guiducci et al., 2019; Lin et al., 2019). Our results supplement the molecular mechanism by which canonical RBPs regulate *SHMT2* mRNA stability and reveal the specific pattern of IGF2BP2 recognition of the m⁶A site in the *SHMT2* CDS, in which HOTAIRM1 plays an indispensable role. Accumulating evidence has confirmed that the expression of SHMT2, as a potential oncogenic driver gene (Lee et al., 2014), is markedly elevated in a variety of cancers (Xie and Pei, 2021), such as lung cancer (DeNicola et al., 2015) and breast cancer (Lie et al., 2020), in which HOTAIRM1 is also highly expressed. However, in some digestive system tumors, the expression of SHMT2 and HOTAIRM1 is not positively correlated. We speculate that this may be related to the reliance of these tumors on cytosolic one-carbon flux and the SLC19A1 expression (Lee et al., 2021). Some studies have also found that loss of the catalytic activity of SHMT2 leads to defective oxidative phosphorylation because of impaired mitochondrial translation (Minton et al., 2018; Morscher et al., 2018), which confirmed our finding that targeting HOTAIRM1 inhibited mitochondrial activity by reducing SHMT2 expression.

Interestingly, HOTAIRM1 was found to be upregulated 54.6-fold in early differentiated neurons (Lin et al., 2011), and to modulate neuron maturation and differentiation (Rea et al., 2020; Cui et al., 2021). Embryonic lncRNAs, which are reactivated in malignant tumors, are likely to play an important role in cancer progression. It has been reported that neurons can release serine into the tumor microenvironment through their axons and promote tumor growth (Banh et al., 2020). This finding indicates that the regulatory effect of HOTAIRM1 on serine metabolism may also affect the metabolic reprogramming of the glioma neural circuit and microenvironment. In evaluating the underlying genetic impact of GBM on the HOTAIRM1 status, we also observed a correlation between the HOTAIRM1 expression level and the IDH mutation status, which has been reported across different datasets (Zhang et al., 2015). According to our results, the expression of HOTAIRM1 in IDH1 mutant samples was indeed lower than that in IDH1 wild-type samples, but the IDH1-R132H mutation did not inhibit the expression of HOTAIRM1, and knockdown of HOTAIRM1 did not reduce the expression of wild-type IDH1, suggesting that the regulatory relationship between IDH mutation status and HOTAIRM1 expression remains to be established in GBM cells (Figure S5). We speculate that this may be the result of the interactions of the glioma microenvironment. Ahmadov et al. also evaluated the relationship between the expression level of HOTAIRM1 and the chromosome 7 copy

number status, which is also associated with EGFR amplification, in GBMs (Ahmadov et al., 2021). Based on our data, we proved that PTBP1 and IGF2BP2 are co-regulators of HOTAIRM1 in GBM.

Using transcriptomic, proteomic and metabolomic approaches, we systematically screened and authenticated the significant target gene *SHMT2* and its interacting RBPs PTBP1 and IGF2BP2 in GBM and found that HOTAIRM1 can maintain the homeostasis of serine and one-carbon metabolism in mitochondria. More specifically, PTBP1 and IGF2BP2 can maintain the expression of the two HOTAIRM1 transcript variants. In general, lncRNAs interact with RBPs that function as adaptor proteins and then change the fate of the bound RNAs (Briata and Gherzi, 2020; Dangelmaier and Lal, 2020). Here, we reveal the vital roles of the two RBPs PTBP1 and IGF2BP2 in the regulation of *SHMT2* by HOTAIRM1. Using the eCLIP-seq method, we identified the sites where PTBP1 and IGF2BP2 proteins bind to *SHMT2* mRNA in A172 glioma cells. RBPs and PTBP1 can bind to many of the same genes, but few of these target genes are coregulated (Van Nostrand et al., 2020). On the online ENCORI platform, we can search the high-stringency CLIP-seq data for the interactions of IGF2BP2 and PTBP1 with *SHMT2* mRNA, and the findings support our results. We also confirmed the eCLIP results by RIP-qPCR and biotin pulldown experiments. The binding region identified in the biotin pulldown assay was not very consistent with the peak position identified by eCLIP-seq. We considered that this may be because the cloned fragment RNA probe changes the structure of the full-length RNA, resulting in different affinities for RBPs. In particular, the presence of HOTAIRM1 maintains the binding of PTBP1 and IGF2BP2 proteins to *SHMT2* mRNA. As an important splicing regulator, PTBP1 can not only participate in mRNA splicing (Ramos et al., 2015) but also regulate lncRNA splicing (Desideri et al., 2020). Our results showed that knockdown of PTBP1 induced the production of unspliced HOTAIRM1 and promoted NMD of *SHMT2* mRNA. Interestingly, HOTAIRM1, as a bridge RNA, recruited PTBP1 and IGF2BP2 together simultaneously. IGF2BP2 modulates mRNA or lncRNA expression by acting as an N⁶-methyladenosine reader (Huang et al., 2018; Hu et al., 2020). lncRNAs can also increase the binding of IGF2BP2 to its target genes to maintain mRNA stability (Wang et al., 2019; Chen et al., 2019). In our study, we revealed a new mechanism by which IGF2BP2 can stabilize HOTAIRM1. Then, HOTAIRM1 increases the recruitment of IGF2BP2 to *SHMT2*, and finally promotes the expression of *SHMT2* through recognition of the m⁶A site.

We also found that the adaptor proteins of HOTAIRM1, i.e., PTBP1 and IGF2BP2, are also RBPs highly expressed in GBM (Jin et al., 2000; Mu et al., 2015). Simultaneously, similar to HOTAIRM1 expression, PTBP1 is expressed at high levels in the mammalian fetal brain (Lilleväli et al., 2001), and IGF2BP2 is also enriched in early-stage neural precursor cells (Fujii et al., 2013). IGF2BP2 can promote mitochondrial oxygen consumption (Janiszewska et al., 2012). PTBP1 has previously been reported to mediate metabolic reprogramming of oxidative phosphorylation to glycolysis (He et al., 2014). We proved that PTBP1 can also maintain mitochondrial oxidative phosphorylation by regulating *SHMT2* expression and cooperates with IGF2BP2 through the HOTAIRM1 bridge in GBM cells. According to the above results, HOTAIRM1 can be used not only as a new marker for GBM molecular typing but also as a molecular target to improve the treatment of GBM. Metabolic therapy targeting *SHMT2* may provide new hope for improving the prognosis of GBM patients.

Limitations of the study

Our research model was based on the culture conditions of conventional oxygen concentration. Whether HOTAIRM1 regulates *SHMT2* expression by hypoxia was not investigated. The specific molecular mechanism of PTBP1 regulating HOTAIRM1 and *SHMT2* needs to be further studied. The specific differences between the two transcripts of HOTAIRM1 in function and mechanism also require further exploration. We preliminarily explored the regulatory relationship between IDH1 and HOTAIRM1, but in order to clarify the regulatory effect of IDH1 on HOTAIRM1 or *SHMT2*, more experimental evidence is needed.

STAR★METHODS

Detailed methods are provided in the online version of this paper and include the following:

- [KEY RESOURCES TABLE](#)
- [RESOURCE AVAILABILITY](#)
 - Lead contact
 - Materials availability

- Data and code availability
- **EXPERIMENTAL MODEL AND SUBJECT DETAILS**
 - Cell culture
 - Mice
 - Patient samples
- **METHOD DETAILS**
 - Cell culture and viral transduction
 - siRNA and plasmid transfection
 - RT-PCR and PCR
 - Real-time PCR
 - Western blot analysis
 - Cell proliferation assays
 - Cell migration and invasion assays
 - Mitochondrial and cytosolic fractionation
 - RNA fluorescence *in situ* hybridization
 - Seahorse assays
 - *In vivo* mouse models
 - Dual luciferase promoter reporter assay
 - Enhanced CLIP-seq
 - Ribonucleoprotein immunoprecipitation
 - Biotin pulldown
 - Protein immunoprecipitation assay
 - RNA stability
 - Methylated RNA immunoprecipitation
 - LncRNA microarray analysis
 - Protein silver staining and mass spectrometry
 - Metabonomic analysis
- **QUANTIFICATION AND STATISTICAL ANALYSIS**

SUPPLEMENTAL INFORMATION

Supplemental information can be found online at <https://doi.org/10.1016/j.isci.2022.104823>.

ACKNOWLEDGMENTS

We gratefully acknowledge contributions from the CGGA and TCGA databases and thank Department of Neurosurgery, Beijing Tiantan Hospital for providing the glioma samples and related anonymous clinical data. We are also grateful to Wei Liu of the Department of Human Anatomy, Histology and Embryology, Institute of Basic Medical Sciences, Chinese Academy of Medical Sciences, for the control brain tissues. This work was supported by the CAMS Innovation Fund for Medical Sciences (CIFMS) grant (2021-I2M-1-034), the National Sciences Foundation of China (82173373, 31671316, 21874156), and the Beijing Nova Program of Science and Technology (Z191100001119137).

AUTHOR CONTRIBUTIONS

W.H. designed and performed most of the experiments with assistance from S.S.W.; Y.J.Q., F.W., and N.Y.T. conducted part of the biological function study, constructed the vectors and performed the bioinformatics analysis; B.Q.Q. and X.Z.P. supervised the research and analyzed the data. W.H. conceived the study and wrote the manuscript; and W.H., B.Q.Q., and X.Z.P. secured funding for the project. All authors participated in interpreting the results and revising the manuscript.

DECLARATION OF INTERESTS

No potential conflicts of interest were disclosed by the authors.

Received: March 6, 2022

Revised: June 12, 2022

Accepted: July 19, 2022

Published: August 19, 2022

REFERENCES

- Ahmadov, U., Picard, D., Bartl, J., Silginer, M., Trajkovic-Arsic, M., Qin, N., Blümel, L., Wolter, M., Lim, J.K.M., Pauck, D., et al. (2021). The long non-coding RNA HOTAIRM1 promotes tumor aggressiveness and radiotherapy resistance in glioblastoma. *Cell Death Dis.* 12, 885.
- Banh, R.S., Biancur, D.E., Yamamoto, K., Sohn, A.S.W., Walters, B., Kuljanin, M., Gikandi, A., Wang, H., Mancias, J.D., Schneider, R.J., et al. (2020). Neurons release serine to support mRNA translation in pancreatic cancer. *Cell* 183, 1202–1218.e25.
- Bonnay, F., Veloso, A., Steinmann, V., Köcher, T., Abdusselamoglu, M.D., Bajaj, S., Rivelles, E., Landskron, L., Esterbauer, H., Zinzen, R.P., and Knoblich, J.A. (2020). Oxidative metabolism drives immortalization of neural stem cells during tumorigenesis. *Cell* 182, 1490–1507.e19.
- Briata, P., and Gherzi, R. (2020). Long non-coding RNA-ribonucleoprotein networks in the post-transcriptional control of gene expression. *Noncoding RNA* 6, 40.
- Cheng, G., Zhang, Q., Pan, J., Lee, Y., Ouari, O., Hardy, M., Zielonka, M., Myers, C.R., Zielonka, J., Weh, K., et al. (2019). Targeting lisdamine to mitochondria mitigates lung tumorigenesis and brain metastasis. *Nat. Commun.* 10, 2205.
- Cheng, Y., Xie, W., Pickering, B.F., Chu, K.L., Savino, A.M., Yang, X., Luo, H., Nguyen, D.T., Mo, S., Barin, E., et al. (2021). N(6)-Methyladenosine on mRNA facilitates a phase-separated nuclear body that suppresses myeloid leukemic differentiation. *Cancer*. Cell. 39, 958–972.e8.
- Chen, R.X., Chen, X., Xia, L.P., Zhang, J.X., Pan, Z.Z., Ma, X.D., Han, K., Chen, J.W., Judd, J.G., Deas, O., et al. (2019). N(6)-methyladenosine modification of circNSUN2 facilitates cytoplasmic export and stabilizes HMGGA2 to promote colorectal liver metastasis. *Nat. Commun.* 10, 4695.
- Chen, Y., Wu, J.J., Lin, X.B., Bao, Y., Chen, Z.H., Zhang, C.R., Cai, Z., Zhou, J.Y., Ding, M.H., Wu, X.J., et al. (2015). Differential lncRNA expression profiles in recurrent gliomas compared with primary gliomas identified by microarray analysis. *Int. J. Clin. Exp. Med.* 8, 5033–5043.
- Chen, Z.H., Wang, W.T., Huang, W., Fang, K., Sun, Y.M., Liu, S.R., Luo, X.Q., and Chen, Y.Q. (2017). The lncRNA HOTAIRM1 regulates the degradation of PML-RARA oncoprotein and myeloid cell differentiation by enhancing the autophagy pathway. *Cell. Death. Differ.* 24, 212–224.
- Cheung, H.C., Hai, T., Zhu, W., Baggerly, K.A., Tsavachidis, S., Krahe, R., and Cote, G.J. (2009). Splicing factors PTBP1 and PTBP2 promote proliferation and migration of glioma cell lines. *Brain* 132, 2277–2288.
- Conway, A.E., Van Nostrand, E.L., Pratt, G.A., Aigner, S., Wilbert, M.L., Sundararaman, B., Freese, P., Lambert, N.J., Sathe, S., Liang, T.Y., et al. (2016). Enhanced CLIP uncovers IMP protein-RNA targets in human pluripotent stem cells important for cell adhesion and survival. *Cell Rep.* 15, 666–679.
- Cui, X., Pertile, R.A.N., Du, Z., Wei, W., Sun, Z., Eyles, D.W., and Kesby, J.P. (2021). Developmental inhibition of long intergenic non-coding RNA, HOTAIRM1, impairs dopamine neuron differentiation and maturation. *Int. J. Mol. Sci.* 22, 7268.
- Dangelmaier, E., and Lal, A. (2020). Adaptor proteins in long noncoding RNA biology. *Biochim. Biophys. Acta. Gene Regul. Mech.* 1863, 194370.
- DeNicola, G.M., Chen, P.H., Mullarky, E., Sudderth, J.A., Hu, Z., Wu, D., Tang, H., Xie, Y., Asara, J.M., Huffman, K.E., et al. (2015). NRF2 regulates serine biosynthesis in non-small cell lung cancer. *Nat. Genet.* 47, 1475–1481.
- Derrien, T., Johnson, R., Bussotti, G., Tanzer, A., Djebali, S., Tilgner, H., Guernec, G., Martin, D., Merkel, A., Knowles, D.G., et al. (2012). The GENCODE v7 catalog of human long noncoding RNAs: analysis of their gene structure, evolution, and expression. *Genome Res.* 22, 1775–1789.
- Desideri, F., Cipriano, A., Petrezselyova, S., Buonaiuto, G., Santini, T., Kasperek, P., Prochazka, J., Janson, G., Paiardini, A., Calicchio, A., et al. (2020). Intronic determinants coordinate charme lncRNA nuclear activity through the interaction with MATR3 and PTBP1. *Cell Rep.* 33, 108548.
- Ellis, B.C., Graham, L.D., and Molloy, P.L. (2014). CRNDE, a long non-coding RNA responsive to insulin/IGF signaling, regulates genes involved in central metabolism. *Biochim. Biophys. Acta.* 1843, 372–386.
- Engel, A.L., Lorenz, N.I., Klann, K., Münch, C., Depner, C., Steinbach, J.P., Ronellenfitch, M.W., and Luger, A.L. (2020). Serine-dependent redox homeostasis regulates glioblastoma cell survival. *Br. J. Cancer.* 122, 1391–1398.
- Frezza, C. (2016). Cancer metabolism: addicted to serine. *Nat. Chem. Biol.* 12, 389–390.
- Fujii, Y., Kishi, Y., and Gotoh, Y. (2013). IMP2 regulates differentiation potentials of mouse neocortical neural precursor cells. *Gene. Cell.* 18, 79–89.
- Guiducci, G., Paone, A., Tramonti, A., Giardina, G., Rinaldo, S., Bouzidi, A., Magnifico, M.C., Marani, M., Menendez, J.A., Fatica, A., et al. (2019). The moonlighting RNA-binding activity of cytosolic serine hydroxymethyltransferase contributes to control compartmentalization of serine metabolism. *Nucleic. Acids. Res.* 47, 4240–4254.
- Haggerty, T.J., Zeller, K.I., Osthus, R.C., Womsey, D.R., and Dang, C.V. (2003). A strategy for identifying transcription factor binding sites reveals two classes of genomic c-Myc target sites. *Proc. Natl. Acad. Sci. USA* 100, 5313–5318.
- Hamilton, M.J., Young, M., Jang, K., Sauer, S., Neang, V.E., King, A.T., Girke, T., and Martinez, E. (2020). HOTAIRM1 lncRNA is downregulated in clear cell renal cell carcinoma and inhibits the hypoxia pathway. *Cancer. Lett.* 472, 50–58.
- Hebbring, S.J., Chai, Y., Ji, Y., Abo, R.P., Jenkins, G.D., Fridley, B., Zhang, J., Eckloff, B.W., Wieben, E.D., and Weinshilboum, R.M. (2012). Serine hydroxymethyltransferase 1 and 2: gene sequence variation and functional genomic characterization. *J. Neurochem.* 120, 881–890.
- He, X., Arslan, A.D., Ho, T.T., Yuan, C., Stampfer, M.R., and Beck, W.T. (2014). Involvement of polypyrimidine tract-binding protein (PTBP1) in maintaining breast cancer cell growth and malignant properties. *Oncogenesis* 3, e84.
- Huang, H., Weng, H., Sun, W., Qin, X., Shi, H., Wu, H., Zhao, B.S., Mesquita, A., Liu, C., Yuan, C.L., et al. (2018). Recognition of RNA N(6)-methyladenosine by IGF2BP proteins enhances mRNA stability and translation. *Nat. Cell Biol.* 20, 285–295.
- Huarte, M. (2015). The emerging role of lncRNAs in cancer. *Nat. Med.* 21, 1253–1261.
- Hu, H., Mu, Q., Bao, Z., Chen, Y., Liu, Y., Chen, J., Wang, K., Wang, Z., Nam, Y., Jiang, B., et al. (2018). Mutational landscape of secondary glioblastoma guides MET-targeted trial in brain tumor. *Cell* 175, 1665–1678.e18.
- Hu, X., Peng, W.X., Zhou, H., Jiang, J., Zhou, X., Huang, D., Mo, Y.Y., and Yang, L. (2020). IGF2BP2 regulates DANCR by serving as an N6-methyladenosine reader. *Cell Death Differ.* 27, 1782–1794.
- Janiszewska, M., Suvà, M.L., Riggi, N., Houtkooper, R.H., Auwerx, J., Clément-Schatlo, V., Radovanovic, I., Rheinbay, E., Provero, P., and Stamenkovic, I. (2012). Imp2 controls oxidative phosphorylation and is crucial for preserving glioblastoma cancer stem cells. *Genes. Dev.* 26, 1926–1944.
- Jiang, T., Nam, D.H., Ram, Z., Poon, W.S., Wang, J., Boldbaatar, D., Mao, Y., Ma, W., Mao, Q., You, Y., et al. (2021). Clinical practice guidelines for the management of adult diffuse gliomas. *Cancer Lett.* 499, 60–72.
- Jin, S., Zhang, X., Miao, Y., Liang, P., Zhu, K., She, Y., Wu, Y., Liu, D.A., Huang, J., Ren, J., and Cui, J. (2018). m(6)A RNA modification controls autophagy through upregulating ULK1 protein abundance. *Cell. Res.* 28, 955–957.
- Jin, W., McCutcheon, I.E., Fuller, G.N., Huang, E.S., and Cote, G.J. (2000). Fibroblast growth factor receptor-1 alpha-exon exclusion and polypyrimidine tract-binding protein in glioblastoma multiforme tumors. *Cancer. Res.* 60, 1221–1224.
- Jin, X., Li, L., Peng, Q., Gan, C., Gao, L., He, S., Tan, S., Pu, W., Liu, Y., Gong, Y., et al. (2022). Glycylrrhethinic acid restricts mitochondrial energy metabolism by targeting SHMT2. *iScience* 25, 104349.
- Kadenbach, B., and Hüttemann, M. (2015). The subunit composition and function of mammalian cytochrome c oxidase. *Mitochondrion* 24, 64–76.
- Kim, D., Fiske, B.P., Birsoy, K., Freinkman, E., Kami, K., Possemato, R.L., Chudnovsky, Y., Pacold, M.E., Chen, W.W., Cantor, J.R., et al. (2015). SHMT2 drives glioma cell survival in ischaemia but imposes a dependence on glycine clearance. *Nature* 520, 363–367.
- Kim, S.H., Lim, K.H., Yang, S., and Joo, J.Y. (2021). Long non-coding RNAs in brain tumors: roles and

- potential as therapeutic targets. *J. Hematol. Oncol.* 14, 77.
- LaGory, E.L., Wu, C., Taniguchi, C.M., Ding, C.K.C., Chi, J.T., von Eyben, R., Scott, D.A., Richardson, A.D., and Giaccia, A.J. (2015). Suppression of PGC-1 α is critical for reprogramming oxidative metabolism in renal cell carcinoma. *Cell Rep.* 12, 116–127.
- LeBleu, V.S., O'Connell, J.T., Gonzalez Herrera, K.N., Wikman, H., Pantel, K., Haigis, M.C., de Carvalho, F.M., Damascena, A., Domingos Chinen, L.T., Rocha, R.M., et al. (2014). PGC-1 α mediates mitochondrial biogenesis and oxidative phosphorylation in cancer cells to promote metastasis. *Nat. Cell Biol.* 16, 992–1003. 1–15.
- Lee, G.Y., Haverty, P.M., Li, L., Kljavin, N.M., Bourgon, R., Lee, J., Stern, H., Modrusan, Z., Seshagiri, S., Zhang, Z., et al. (2014). Comparative oncogenomics identifies PSMB4 and SHMT2 as potential cancer driver genes. *Cancer Res.* 74, 3114–3126.
- Lee, W.D., Pirona, A.C., Sarvin, B., Stern, A., Nevo-Dinur, K., Besser, E., Sarvin, N., Lagziel, S., Mukha, D., Raz, S., et al. (2021). Tumor reliance on cytosolic versus mitochondrial one-carbon flux depends on folate availability. *Cell Metabol.* 33, 190–198.e6.
- Lie, A.M., Ducker, G.S., Li, Y., Seoane, J.A., Xiao, Y., Melemenidis, S., Zhou, Y., Liu, L., Vanharanta, S., Graves, E.E., et al. (2020). Metabolic profiling reveals a dependency of human metastatic breast cancer on mitochondrial serine and one-carbon unit metabolism. *Mol. Cancer Res.* 18, 599–611.
- Liang, Q., Li, X., Guan, G., Xu, X., Chen, C., Cheng, P., Cheng, W., and Wu, A. (2019). Long non-coding RNA, HOTAIRM1, promotes glioma malignancy by forming a ceRNA network. *Aging (Albany NY)* 11, 6805–6838.
- Li, J.H., Liu, S., Zhou, H., Qu, L.H., and Yang, J.H. (2014). starBase v2.0: decoding miRNA-ceRNA, miRNA-ncRNA and protein-RNA interaction networks from large-scale CLIP-Seq data. *Nucleic Acids Res.* 42, D92–D97.
- Lilleväli, K., Kulla, A., and Ord, T. (2001). Comparative expression analysis of the genes encoding polypyrimidine tract binding protein (PTB) and its neural homologue (brPTB) in prenatal and postnatal mouse brain. *Mech. Dev.* 101, 217–220.
- Lin, C., Zhang, Y., Chen, Y., Bai, Y., and Zhang, Y. (2019). Long noncoding RNA LINC01234 promotes serine hydroxymethyltransferase 2 expression and proliferation by competitively binding miR-642a-5p in colon cancer. *Cell Death Dis.* 10, 137.
- Lin, M., Pedrosa, E., Shah, A., Hrabovsky, A., Maqbool, S., Zheng, D., and Lachman, H.M. (2011). RNA-Seq of human neurons derived from iPSC cells reveals candidate long non-coding RNAs involved in neurogenesis and neuropsychiatric disorders. *PLoS One* 6, e23356.
- Li, Q., Dong, C., Cui, J., Wang, Y., and Hong, X. (2018). Over-expressed lncRNA HOTAIRM1 promotes tumor growth and invasion through up-regulating HOXA1 and sequestering G9a/EZH2/Dnmts away from the HOXA1 gene in glioblastoma multiforme. *J. Exp. Clin. Cancer Res.* 37, 265.
- Li, Z., Liu, L., Jiang, S., Li, Q., Feng, C., Du, Q., Zou, D., Xiao, J., Zhang, Z., and Ma, L. (2021). LncExpDB: an expression database of human long non-coding RNAs. *Nucleic Acids Res.* 49, D962–D968.
- Lucas, S., Chen, G., Aras, S., and Wang, J. (2018). Serine catabolism is essential to maintain mitochondrial respiration in mammalian cells. *Life Sci. Alliance* 1, e201800036.
- Marrocco, I., Altieri, F., Rubini, E., Paglia, G., Chichiarelli, S., Giamogante, F., Macone, A., Perugia, G., Magliocca, F.M., Gurtner, A., et al. (2019). Shmt2: a Stat3 signaling new player in prostate cancer energy metabolism. *Cells* 8, 1048.
- Minton, D.R., Nam, M., McLaughlin, D.J., Shin, J., Bayraktar, E.C., Alvarez, S.W., Sviderskiy, V.O., Papagiannakopoulos, T., Sabatini, D.M., Birsoy, K., and Possemato, R. (2018). Serine catabolism by SHMT2 is required for proper mitochondrial translation initiation and maintenance of formyl-methionyl-tRNAs. *Mol. Cell.* 69, 610–621.e5.
- Morscher, R.J., Ducker, G.S., Li, S.H.J., Mayer, J.A., Gitai, Z., Sperl, W., and Rabinowitz, J.D. (2018). Mitochondrial translation requires folate-dependent tRNA methylation. *Nature* 554, 128–132.
- Mu, Q., Wang, L., Yu, F., Gao, H., Lei, T., Li, P., Liu, P., Zheng, X., Hu, X., Chen, Y., et al. (2015). Imp2 regulates GBM progression by activating IGF2/PI3K/Akt pathway. *Cancer Biol. Ther.* 16, 623–633.
- Muthusamy, T., Cordes, T., Handzlik, M.K., You, L., Lim, E.W., Gengatharan, J., Pinto, A.F.M., Badur, M.G., Kolar, M.J., Wallace, M., et al. (2020). Serine restriction alters sphingolipid diversity to constrain tumour growth. *Nature* 586, 790–795.
- Nikiforov, M.A., Chandriani, S., O'Connell, B., Petrenko, O., Kottenko, I., Beavis, A., Sedivy, J.M., and Cole, M.D. (2002). A functional screen for Myc-responsive genes reveals serine hydroxymethyltransferase, a major source of the one-carbon unit for cell metabolism. *Mol. Cell Biol.* 22, 5793–5800.
- Pacold, M.E., Brimacombe, K.R., Chan, S.H., Rohde, J.M., Lewis, C.A., Swier, L.J.Y.M., Possemato, R., Chen, W.W., Sullivan, L.B., Fiske, B.P., et al. (2016). A PHGDH inhibitor reveals coordination of serine synthesis and one-carbon unit fate. *Nat. Chem. Biol.* 12, 452–458.
- Palazzo, A.F., and Koonin, E.V. (2020). Functional long non-coding RNAs evolve from junk transcripts. *Cell* 183, 1151–1161.
- Patel, V.L., Mitra, S., Harris, R., Buxbaum, A.R., Lionnet, T., Bingerow, M., Girvin, M., Levy, M., Almo, S.C., Singer, R.H., and Chao, J.A. (2012). Spatial arrangement of an RNA zipcode identifies mRNAs under post-transcriptional control. *Genes Dev.* 26, 43–53.
- Peng, Z., Liu, C., and Wu, M. (2018). New insights into long noncoding RNAs and their roles in glioma. *Mol. Cancer* 17, 61.
- Qin, H., Ni, H., Liu, Y., Yuan, Y., Xi, T., Li, X., and Zheng, L. (2020). RNA-binding proteins in tumor progression. *J. Hematol. Oncol.* 13, 90.
- Ramos, A.D., Andersen, R.E., Liu, S.J., Nowakowski, T.J., Hong, S.J., Gertz, C., Salinas, R.D., Zarabi, H., Kriegstein, A.R., and Lim, D.A. (2015). The long noncoding RNA Pnky regulates neuronal differentiation of embryonic and postnatal neural stem cells. *Cell Stem Cell* 16, 439–447.
- Rea, J., Menci, V., Tollis, P., Santini, T., Armaos, A., Garone, M.G., Iberite, F., Cipriano, A., Tartaglia, G.G., Rosa, A., et al. (2020). HOTAIRM1 regulates neuronal differentiation by modulating NEUROGENIN 2 and the downstream neurogenic cascade. *Cell Death Dis.* 11, 527.
- Statello, L., Guo, C.J., Chen, L.L., and Huarte, M. (2021). Gene regulation by long non-coding RNAs and its biological functions. *Nat. Rev. Mol. Cell Biol.* 22, 96–118.
- Suvasini, R., Shruti, B., Thota, B., Shinde, S.V., Friedmann-Morvinski, D., Nawaz, Z., Prasanna, K.V., Thennarasu, K., Hegde, A.S., Arivazhagan, A., et al. (2011). Insulin growth factor-2 binding protein 3 (IGFBP3) is a glioblastoma-specific marker that activates phosphatidylinositol 3-kinase/mitogen-activated protein kinase (PI3K/MAPK) pathways by modulating IGF-2. *J. Biol. Chem.* 286, 25882–25890.
- Tan, A.C., Ashley, D.M., López, G.Y., Malinzak, M., Friedman, H.S., and Khasraw, M. (2020). Management of glioblastoma: state of the art and future directions. *CA. Cancer J. Clin.* 70, 299–312.
- Tang, Z., Li, C., Kang, B., Gao, G., Li, C., and Zhang, Z. (2017). GEPIA: a web server for cancer and normal gene expression profiling and interactive analyses. *Nucleic Acids Res.* 45, W98–W102.
- Tian, X., Ma, J., Wang, T., Tian, J., Zhang, Y., Mao, L., Xu, H., and Wang, S. (2018). Long non-coding RNA HOXA transcript antisense RNA myeloid-specific 1-HOXA1 Axis downregulates the immunosuppressive activity of myeloid-derived suppressor cells in lung cancer. *Front. Immunol.* 9, 473.
- Tiwari, V., Daoud, E.V., Hatanpaa, K.J., Gao, A., Zhang, S., An, Z., Ganji, S.K., Raisanen, J.M., Lewis, C.M., Askari, P., et al. (2020). Glycine by MR spectroscopy is an imaging biomarker of glioma aggressiveness. *Neuro Oncol.* 22, 1018–1029.
- Uszczynska-Ratajczak, B., Lagarde, J., Frankish, A., Guigó, R., and Johnson, R. (2018). Towards a complete map of the human long non-coding RNA transcriptome. *Nat. Rev. Genet.* 19, 535–548.
- Van Meir, E.G., Hadjipanayis, C.G., Norden, A.D., Shu, H.K., Wen, P.Y., and Olson, J.J. (2010). Exciting new advances in neuro-oncology: the avenue to a cure for malignant glioma. *CA. Cancer J. Clin.* 60, 166–193.
- Van Nostrand, E.L., Freese, P., Pratt, G.A., Wang, X., Wei, X., Xiao, R., Blue, S.M., Chen, J.Y., Cody, N.A.L., Dominguez, D., et al. (2020). A large-scale binding and functional map of human RNA-binding proteins. *Nature* 583, 711–719.
- Van Nostrand, E.L., Pratt, G.A., Shishkin, A.A., Gelboin-Burkhart, C., Fang, M.Y., Sundararaman,

- B., Blue, S.M., Nguyen, T.B., Surka, C., Elkins, K., et al. (2016). Robust transcriptome-wide discovery of RNA-binding protein binding sites with enhanced CLIP (eCLIP). *Nat. Methods* 13, 508–514.
- Wang, B., Wang, W., Zhu, Z., Zhang, X., Tang, F., Wang, D., Liu, X., Yan, X., and Zhuang, H. (2017). Mitochondrial serine hydroxymethyltransferase 2 is a potential diagnostic and prognostic biomarker for human glioma. *Clin. Neurol. Neurosurg.* 154, 28–33.
- Wang, H., Li, H., Jiang, Q., Dong, X., Li, S., Cheng, S., Shi, J., Liu, L., Qian, Z., and Dong, J. (2021). HOTAIRM1 promotes malignant progression of transformed fibroblasts in glioma stem-like cells remodeled microenvironment via regulating miR-133b-3p/TGFbeta Axis. *Front. Oncol.* 11, 603128.
- Wang, R.J., Li, J.W., Bao, B.H., Wu, H.C., Du, Z.H., Su, J.L., Zhang, M.H., and Liang, H.Q. (2015). MicroRNA-873 (miRNA-873) inhibits glioblastoma tumorigenesis and metastasis by suppressing the expression of IGF2BP1. *J. Biol. Chem.* 290, 8938–8948.
- Wang, Y., Lu, J.H., Wu, Q.N., Jin, Y., Wang, D.S., Chen, Y.X., Liu, J., Luo, X.J., Meng, Q., Pu, H.Y., et al. (2019). LncRNA LINRIS stabilizes IGF2BP2 and promotes the aerobic glycolysis in colorectal cancer. *Mol. Cancer* 18, 174.
- Wan, L., Kong, J., Tang, J., Wu, Y., Xu, E., Lai, M., and Zhang, H. (2016). HOTAIRM1 as a potential biomarker for diagnosis of colorectal cancer functions the role in the tumour suppressor. *J. Cell. Mol. Med.* 20, 2036–2044.
- Wei, S., Zhao, M., Wang, X., Li, Y., and Wang, K. (2016). PU.1 controls the expression of long noncoding RNA HOTAIRM1 during granulocytic differentiation. *J. Hematol. Oncol.* 9, 44.
- Wei, Z., Song, J., Wang, G., Cui, X., Zheng, J., Tang, Y., Chen, X., Li, J., Cui, L., Liu, C.Y., and Yu, W. (2018). Deacetylation of serine hydroxymethyltransferase 2 by SIRT3 promotes colorectal carcinogenesis. *Nat. Commun.* 9, 4468.
- Xia, H., Liu, Y., Wang, Z., Zhang, W., Qi, M., Qi, B., and Jiang, X. (2020). Long noncoding RNA HOTAIRM1 maintains tumorigenicity of glioblastoma stem-like cells through regulation of HOX gene expression. *Neurotherapeutics* 17, 754–764.
- Xie, M., and Pei, D.S. (2021). Serine hydroxymethyltransferase 2: a novel target for human cancer therapy. *Invest. N. Drugs.* 39, 1671–1681.
- Xie, Q., Wu, Q., Horbinski, C.M., Flavahan, W.A., Yang, K., Zhou, W., Dombrowski, S.M., Huang, Z., Fang, X., Shi, Y., et al. (2015). Mitochondrial control by DRP1 in brain tumor initiating cells. *Nat. Neurosci.* 18, 501–510.
- Yamada, T., Imamachi, N., Onoguchi-Mizutani, R., Imamura, K., Suzuki, Y., and Akimitsu, N. (2018). 5'-Bromouridine IP chase (BRIC)-Seq to determine RNA half-lives. *Methods. Mol. Biol.* 1720, 1–13.
- Yang, L., Garcia Canaveras, J.C., Chen, Z., Wang, L., Liang, L., Jang, C., Mayr, J.A., Zhang, Z., Ghergurovich, J.M., Zhan, L., et al. (2020). Serine catabolism feeds NADH when respiration is impaired. *Cell Metabol.* 31, 809–821.e6.
- Yang, X., Wang, Z., Li, X., Liu, B., Liu, M., Liu, L., Chen, S., Ren, M., Wang, Y., Yu, M., et al. (2018). SHMT2 desuccinylation by SIRT5 drives cancer cell proliferation. *Cancer Res.* 78, 372–386.
- Yao, R.W., Wang, Y., and Chen, L.L. (2019). Cellular functions of long noncoding RNAs. *Nat. Cell. Biol.* 21, 542–551.
- Ye, J., Fan, J., Venneti, S., Wan, Y.W., Pawel, B.R., Zhang, J., Finley, L.W.S., Lu, C., Lindsten, T., Cross, J.R., et al. (2014). Serine catabolism regulates mitochondrial redox control during hypoxia. *Cancer Discov.* 4, 1406–1417.
- Yu, H., Lindsay, J., Feng, Z.P., Frankenberg, S., Hu, Y., Carone, D., Shaw, G., Pask, A.J., O'Neill, R., Papenfuss, A.T., and Renfree, M.B. (2012). Evolution of coding and non-coding genes in HOX clusters of a marsupial. *BMC. Genom.* 13, 251.
- Zhang, X., Lian, Z., Padden, C., Gerstein, M.B., Rozowsky, J., Snyder, M., Gingeras, T.R., Kapranov, P., Weissman, S.M., and Newburger, P.E. (2009). A myelopoiesis-associated regulatory intergenic noncoding RNA transcript within the human HOXA cluster. *Blood* 113, 2526–2534.
- Zhang, X.Q., and Leung, G.K.K. (2014). Long non-coding RNAs in glioma: functional roles and clinical perspectives. *Neurochem. Int.* 77, 78–85.
- Zhang, X.Q., Kiang, K.M.Y., Wang, Y.C., Pu, J.K.S., Ho, A., Cheng, S.Y., Lee, D., Zhang, P.D., Chen, J.J., Lui, W.M., et al. (2015). IDH1 mutation-associated long non-coding RNA expression profile changes in glioma. *J. Neuro Oncol.* 125, 253–263.
- Zhang, X., Sun, S., Pu, J.K.S., Tsang, A.C.O., Lee, D., Man, V.O.Y., Lui, W.M., Wong, S.T.S., and Leung, G.K.K. (2012). Long non-coding RNA expression profiles predict clinical phenotypes in glioma. *Neurobiol. Dis.* 48, 1–8.
- Zhang, X., Weissman, S.M., and Newburger, P.E. (2014). Long intergenic non-coding RNA HOTAIRM1 regulates cell cycle progression during myeloid maturation in NB4 human promyelocytic leukemia cells. *RNA Biol.* 11, 777–787.
- Zhang, Y., Liu, Z., Wang, X., Jian, H., Xiao, H., and Wen, T. (2022). SHMT2 promotes cell viability and inhibits ROS-dependent, mitochondrial-mediated apoptosis via the intrinsic signaling pathway in bladder cancer cells. *Cancer. Gene. Ther.* <https://doi.org/10.1038/s41417-022-00470-5>.
- Zhao, L.N., Björklund, M., Caldez, M.J., Zheng, J., and Kaldis, P. (2021). Therapeutic targeting of the mitochondrial one-carbon pathway: perspectives, pitfalls, and potential. *Oncogene* 40, 2339–2354.
- Zhu, L., Wei, Q., Qi, Y., Ruan, X., Wu, F., Li, L., Zhou, J., Liu, W., Jiang, T., Zhang, J., et al. (2019). PTB-AS, a novel natural antisense transcript, P promotes glioma progression by improving PTBP1 mRNA stability with SND1. *Mol. Ther.* 27, 1621–1637.

STAR★METHODS

KEY RESOURCES TABLE

REAGENT or RESOURCE	SOURCE	IDENTIFIER
Antibodies		
β-Actin (AC-15) Mouse monoclonal antibody	Sigma-Aldrich	# A5441; RRID: AB_476744
CDH23 Rabbit polyclonal antibody	ABclonal Technology Co.	# A2785; RRID: AB_2764627
CYP26B1 Rabbit polyclonal antibody	Aviva Systems Biology	# ARP57351_P050; RRID: AB_10645178
RPS6KA2 Rabbit polyclonal antibody	Aviva Systems Biology	# ARP56170_P050; RRID: AB_2047872
GPR56 Rabbit polyclonal antibody	Aviva Systems Biology	# ARP58627_P050; RRID: AB_2046021
CALCRL Rabbit polyclonal antibody	Aviva Systems Biology	# ARP42260_P050; RRID: AB_2045267
PDHX Rabbit polyclonal antibody	Bioworld Technology	# BS8207; RRID: AB_2922946
SENP2 Rabbit polyclonal antibody	Bioworld Technology	# BS1470; RRID: AB_1663282
MMP-16 Rabbit polyclonal antibody	Bioworld Technology	# BS1234; RRID: AB_1663255
PRTFDC1 Rabbit polyclonal antibody	ABclonal Technology Co.	# A4875; RRID: AB_2765913
GNAQ Rabbit polyclonal antibody	Abcepta Biotech Ltd. Co.	# AP14179a; RRID: AB_11136994
DIAPH1 Rabbit polyclonal antibody	ABclonal Technology Co.	# A5772; RRID: AB_2766526
TJP1/ZO-1 (D7D12) Rabbit monoclonal antibody	Cell Signaling Technology	# 8193S; RRID: AB_10898025
SERPINE1 (C-20) Goat polyclonal antibody	Santa Cruz Biotechnology	# sc-6642; RRID: AB_2186887
NRAS (F155) Mouse monoclonal antibody	Santa Cruz Biotechnology	# sc-31; RRID: AB_628041
SHMT2 Rabbit polyclonal antibody	ABclonal Technology Co.	# A1215; RRID: AB_2759037
SHMT2 Rabbit monoclonal antibody	Cell Signaling Technology	# 12762S; RRID: AB_2798018
SHMT1 Rabbit polyclonal antibody	ABclonal Technology Co.	# A4113; RRID: AB_2765507
PTBP1 RIP-Certified Rabbit polyclonal antibody	Medical & Biological Laboratories	# RN011P; RRID: AB_1570645
IGF2BP1 RIP-Certified Rabbit polyclonal antibody	Medical & Biological Laboratories	# RN007P; RRID: AB_1570640
IGF2BP2 RIP-Certified Rabbit polyclonal antibody	Medical & Biological Laboratories	# RN008P; RRID: AB_1570641
IGF2BP3 RIP-Certified Rabbit polyclonal antibody	Medical & Biological Laboratories	# RN009P; RRID: AB_1570642
PCBP2 RIP-Certified Rabbit polyclonal antibody	Medical & Biological Laboratories	# RN025P; RRID: AB_1953052
TP53 (DO-1) Mouse monoclonal antibody	Santa Cruz Biotechnology	# sc-126; RRID: AB_628082
FLAG Rabbit polyclonal antibody	Sigma-Aldrich	#F7425; RRID: AB_439687
COX-4 Mouse monoclonal antibody	Bioworld Technology	# MB0102; RRID: AB_2922947
N-Myc (B8.4.B) Mouse monoclonal antibody	Santa Cruz Biotechnology	# sc-53993; RRID: AB_831602
C-Myc (9E10) Mouse monoclonal antibody	Santa Cruz Biotechnology	# sc-40; RRID: AB_627268
HIF-1α Mouse monoclonal antibody	Abcam	# ab16066; RRID: AB_302234
PHGDH Rabbit polyclonal antibody	ABclonal Technology Co.	# A4617; RRID: AB_2765787
IDH1 Rabbit polyclonal antibody	Cell Signaling Technology	# 3997; RRID: AB_1904011
IDH2 (5F11) Mouse monoclonal antibody	Abcam	# ab55271; RRID: AB_943793
IDH1 (R132H) Mouse monoclonal antibody	Dianova	# DIA-H09; RRID: AB_2335716
Horseradish peroxidase labeled Goat anti-mouse IgG	ZSGB-Bio	# ZB-2305; RRID: AB_2747415

(Continued on next page)

Continued

REAGENT or RESOURCE	SOURCE	IDENTIFIER
Horseradish peroxidase labeled Goat anti-rabbit IgG	ZSGB-Bio	# ZB-2301; RRID: AB_2747412
Horseradish peroxidase labeled Rabbit anti-goat IgG	ZSGB-Bio	# ZB-2306; RRID: AB_2868454

Biological samples

Control brain	The human brain bank of the Institute of Basic Medical Sciences, Chinese Academy of Medical Sciences	PTB001
		PTB002
		PTB003
		PTB004
		PTB005
		PTB006

Chemicals, peptides, and recombinant proteins

MTS Reagent Powder	Promega	#G1112
Phenazine methosulfate	Sigma-Aldrich	#P9625
INTERFERin siRNA Transfection Reagent	Polyplus	# 409-10
SYBR Premix Ex Taq	Takara	# RR420A
Penicillin-Streptomycin Solution	HyClone	# SV30010
PBS	Gibco	# 10,010-023
DMEM/HIGH Glucose	HyClone	# SH30022-01
Astrocyte Medium	ScienCell	# 1801
Puromycin	Gibco	# A1113803
FuGENE® 6 Transfection Reagent	Promega	#E2691
Halt™ Protease Inhibitor Cocktail (100X)	Thermo Scientific	# 78,430
Phanta Max Super-Fidelity DNA Polymerase	Vazyme	#P505-d1
0.1% tween 20	VWR Chemicals	# 9005-64-5
SuperSignal™ West Pico PLUS kit	Thermo Scientific	# 34,580
Matrigel Matix	BD BioCoat	# 354,234
RNaseA	TIANGEN	# RT405-12
TRIzol	Invitrogen	# 15,596,018
Digoxigenin RNA labeling mix	Roche	# 11,277,073,910
TSA™ Plus Fluorescein System	PerkinElmer	# NEL741001KT
Anti-Digoxigenin-POD	Roche	# 11,207,733,910
4-thiouridine	Sigma-Aldrich	#T4509
Tris-HCl pH7.4	Solarbio	#T1090
NaCl	Invitrogen	# AM9759
SDS	VWR Chemicals	# 0227
Sodium deoxycholate	Sigma-Aldrich	#D6750
DTT	Gibco	#P2325
200 × protease inhibitor cocktail III	Calbiochem/Merck	# 539,134-1SET
RNase inhibitor	Promega	#N2515
RNase I	Invitrogen	# AM2295
Protein A Dynabeads	Invitrogen	# 10002D
Proteinase K	New England Biolabs	#P8107S
SeaKem GTG Agarose	Lonza	# 50,070
Protein A-agarose beads	Roche	# 11,719,408,001
T7 RNA polymerase	Takara	# 2540B

(Continued on next page)

Continued

REAGENT or RESOURCE	SOURCE	IDENTIFIER
Biotin RNA Labeling Mix	Roche	# 11,685,597,910
Streptavidin Sepharose	GE	# 17-5113-01
HEPES	Gibco	# 15,630-080
KCl	Invitrogen	# AM9640G
NP40	Sigma-Aldrich	# NP40S
MgCl ₂	Invitrogen	# AM9530G
EDTA	Invitrogen	# AM9260G
Ribonucleoside Vanadyl Complex	New England Biolabs	#S1402S
tRNA from Ecoli	Sigma-Aldrich	#R1753
Fetal Bovine Serum	Biowest	#S1580-500
100 bp DNA Ladder	Vazyme	# MD104-01

Critical commercial assays

RIP-Assay Kit	MBL Beijing Biotech Co., LTD	# RN1001
BRIC Kit	MBL Beijing Biotech Co., LTD	# RN1007/1008
Magna MeRIP™ m6A Kit	Sigma-Aldrich	# 17-10499
RNeasy Mini Kit	QIAGEN	# 74,106
Endo-Free Plasmid Maxi Kit	QIAGEN	# 13,262
Trans-Script First-Strand cDNA Synthesis Super-Mix	Trans-Gen Biotech.	# AT301-02
HiScript II Q RT Super-Mix for qPCR (+gDNA wiper)	Vazyme	#R223-01
XF cell mito stress test kit	Seahorse Bioscience	# 101,848-400
Cell Mitochondria Isolation Kit	Beyotime	#C3601
Dual-Luciferase® Reporter Assay System	Promega	#E1960
NE-PER Extraction Reagent	Thermo Fisher Scientific	# 78,835
Pierce Classic IP Kit	Thermo Fisher Scientific	# 26,146
RNA Clean & Concentrator-5	Zymo Research	#R1016

Deposited data

The HOTAIRM1 knockdown microarray data and the eCLIP-seq data are deposited at GEO	This paper	GEO: GSE192627; GEO: GSE192792
--	------------	--------------------------------

Experimental models: Celllines

Human GBM cell: A172	ATCC	# CRL-1620
Human GBM cell: U87MG	ATCC	# HTB-14
Human GBM cell: T98G	ATCC	# CRL-1690
Human GBM cell: LN-18	ATCC	# CRL-2610
Human GBM cell: LN-229	ATCC	# CRL-2611
Human GBM cell: U-118MG	ATCC	# HTB-15
Human GBM cell: U-138MG	ATCC	# HTB-16
Human glioma cell: CCF-STTG1	ATCC	# CRL-1718
Human glioma cell: H4	ATCC	# HTB-148
Human glioma cell: U251	the Cell Center of Peking Union Medical College	# 3101HUMTCHU58
Human glioma cell: TJ905	the Cell Center of Peking Union Medical College	# 1101HUM-PUMC000267
Human glioma cell: Hs683	the Cell Center of Peking Union Medical College	# 1101HUM-PUMC000345

(Continued on next page)

Continued

REAGENT or RESOURCE	SOURCE	IDENTIFIER
Human glioma cell: SF-126	the Cell Center of Peking Union Medical College	# 1101HUM-PUMC000049
Human glioma cell: SF-763	the Cell Center of Peking Union Medical College	# 1101HUM-PUMC000050
Human glioma cell: SF-767	the Cell Center of Peking Union Medical College	# 1101HUM-PUMC000051
Human glioma cell: SHG-44	The National Collection of Authenticated Cell Cultures	# TCHu 48
Normal human astrocyte cell: NHA	Lonza	# CC-2565
Human astrocyte cell (from cerebral cortex): HA	Sciencell	# 1800
Human astrocyte cell (from cerebellar): HAc	Sciencell	# 1810
Human astrocyte cell (from spinal cord): HAsp	Sciencell	# 1820
Experimental models: Organisms/strains		
BALB/c nude mice	Beijing Vital River Laboratory	N/A
Oligonucleotides		
siRNA-1 HOTAIRM1 (siHOTAIRM1-1): CCTTTGCTGTTAAGAGCCAGGTTCT	Shanghai GenePharma Co., Ltd	N/A
siRNA-2 HOTAIRM1: CACATGTTGCTTACATGCTGCGTTT	Shanghai GenePharma Co., Ltd	N/A
siRNA-3 HOTAIRM1: AAGATGAACTGGCGAGAGGTCTGTT	Shanghai GenePharma Co., Ltd	N/A
siRNA-4 HOTAIRM1 (siHOTAIRM1-2): AGATGAACTGGCGAGAGGTCTGTTT	Shanghai GenePharma Co., Ltd	N/A
siRNA-5 HOTAIRM1 (siHOTAIRM1-1/2): AGAAACTCCGTGTTACTCATT	Shanghai GenePharma Co., Ltd	N/A
shNT (shRNA lentivirus negative control vector): hU6-MCS-Ubiquitin-EGFP-IRES-puromycin TTCTCCGAACGTGTCACGT	GeneChem	GV248, con077
shHOTAIRM1: AGAAACTCCGTGTTACTCATT	GeneChem	52,745-1
shHOTAIRM1: GGAGACTGGTAGCTTATTTAAA	GeneChem	52,746-11
shSHMT2 GTCTGACGTC AAGCGGATATC	GeneChem	72,467-1
siPTBP1-1 AGAAGGACCGCAAGAUGGCACUGAU	Shanghai GenePharma Co., Ltd	N/A
siPTBP1-2 ACCGCAAGAUGGCACUGAUCCAGAU	Shanghai GenePharma Co., Ltd	N/A
siPTBP1-3 AGACCAGAGATTTTATTTT	Shanghai GenePharma Co., Ltd	N/A
siGF2BP1-1 GCUCCCUAUAGCUCCUUUATT	Shanghai GenePharma Co., Ltd	N/A
siGF2BP1-2 CCGGGAGCAGACCAGGCAATT	Shanghai GenePharma Co., Ltd	N/A
siGF2BP2-1 ACCAAAGTAGCCGAAGAGAT	Shanghai GenePharma Co., Ltd	N/A

(Continued on next page)

Continued

REAGENT or RESOURCE	SOURCE	IDENTIFIER
siGF2BP2-2 CGGAAAGAACCATCACTGT	Shanghai GenePharma Co., Ltd	N/A
siGF2BP3-1 AUAAGUAUACAUUCUCACAG	Shanghai GenePharma Co., Ltd	N/A
siGF2BP3-2 AUUAUACAGCGUCAAUUCCUG	Shanghai GenePharma Co., Ltd	N/A
Recombinant DNA		
LV5-HOTAIRM1-1	Shanghai GenePharma Co., Ltd	170612BZ
LV5-HOTAIRM1-2	Shanghai GenePharma Co., Ltd	170611BZ
LV-SHMT2 (NM_005412)	GeneChem	LVKL21044-1
Software and algorithms		
GraphPad Prism 5	GraphPad software	https://www.graphpad.com/scientific-software/prism/
Seahorse Wave Controller 2.4	Agilent	https://www.agilent.com/
Adobe Photoshop 6.0	Adobe	https://www.adobe.com/cn/products/photoshop.html
IGV_2.8.13	IGV	https://software.broadinstitute.org/software/igv/
Other		
BioTrace nitrocellulose membrane	Pall Corporation	# 66,485
Transwell Polycarbonate Membrane Insert, Sterile	Corning	# 3422
Microsyringe	Hamilton	# 80,383
Magnetic bead collection apparatus	Invitrogen	# 123-21D

RESOURCE AVAILABILITY**Lead contact**

Further information and requests for resources and reagents should be directed to and will be fulfilled by the lead contact, Xiaozhong Peng (pengxiaozhong@pumc.edu.cn).

Materials availability

This study did not generate new unique reagents and all materials mentioned in the manuscript are available from the [lead contact](#) on request.

Data and code availability

Data: The eCLIP-seq and HOTAIRM1 knockdown microarray data reported in this paper have been deposited in the GEO: GSE192792 and GEO: GSE192627.

Code: This paper does not report original code.

Additional information: Any additional information from the data reported in this paper is available from the [lead contact](#) on request.

EXPERIMENTAL MODEL AND SUBJECT DETAILS**Cell culture**

The human glioma cell lines T98G, U87MG, A172, CCF-STTG1, U-118MG, U-138MG, LN-18, LN-229 and H4 were purchased from the AmericanType Culture Collection (ATCC) and cultured according to the guidelines recommended by the ATCC. The U251, Hs683, TJ905, SF126, SF763, and SF767 cell lines (from the Cell Center of Peking Union Medical College) were cultured in minimum essential medium and Iscove's modified Dulbecco's medium supplemented with 10% fetal bovine serum (FBS) and 1%

penicillin/streptomycin. The SHG-44 cell line was ordered from the National Collection of Authenticated Cell Cultures. The normal human astrocyte line NHA was purchased from the Lonza Group and cultured with Clonetics medium and reagents. The other human astrocyte lines HA (from the cerebral cortex), HAc (from the cerebellum), and HAsp (from the spinal cord) were purchased from ScienCell Research Laboratories and cultured with astrocyte medium (catalog no. 1801). All cells were maintained at 37°C in a humidified atmosphere containing 5% CO₂ and were negative for mycoplasma contamination.

Mice

Six-to eight-week-old male BALB/c nu/nu mice (from Beijing Vital River Laboratory) were used to evaluate the inhibitory effect of HOTAIRM1 knockdown *in vivo*. Mice (five per cage) were housed in a conventional barrier facility on a 12 h/12 h light/dark cycle at 22°C for 12 h, with free access to water and food. All animal studies were approved by the IACUC of the Center for Experimental Animal Research (China), and all animal experiments were performed in accordance with institutional guidelines and abided by the declaration of ethical approval for experiments.

Patient samples

Tumor samples from individuals with grade II–IV glioma and the control brain tissues (cerebral autopsy samples from individuals without cancer) were obtained from the Department of Neurosurgery, Beijing Tiantan Hospital and the human brain bank of the Institute of Basic Medical Sciences, Chinese Academy of Medical Sciences. Each sample was snap-frozen in liquid nitrogen. All samples were classified according to the third edition of the WHO Classification of Tumors of the Central Nervous System published in 2000. Informed consent for the use of samples was obtained from all patients before surgery, and approval was obtained from the Medical Ethics Committee of Beijing Tiantan Hospital (Beijing, China).

METHOD DETAILS

Cell culture and viral transduction

The human glioma cell lines T98G, U87MG and A172 were cultured according to the guidelines recommended by ATCC. Construction of the HOTAIRM1 and SHMT2 knockdown plasmids and lentiviruses and packaging of the Flag-SHMT2 overexpression lentiviruses were performed at GeneChem. In addition, HOTAIRM1-1 and HOTAIRM1-2 overexpression lentiviruses were produced at GenePharma. Infected cells were selected with puromycin (A1113803, GIBCO; U87MG: 0.75 µg/mL, T98G: 3 µg/mL, A172: 0.5 µg/mL) for 14 days. The HOTAIRM1-knockdown, SHMT2-knockdown and HOTAIRM1-overexpression lentiviruses expressed green fluorescent protein whereas the SHMT2-overexpression lentivirus expressed red fluorescent protein and a Flag-tagged fusion protein. These fluorescent markers were used to select stably infected cells. Lentiviral particles were added to cells with HiTransG P (1 ×) to increase the efficiency of viral infection. All cells were maintained at 37°C in 5% CO₂.

siRNA and plasmid transfection

The siRNAs for HOTAIRM1, PTBP1, IGF2BP1, IGF2BP2 and IGF2BP3 were synthesized by Shanghai GenePharma Company and transfected into glioma cell lines using INTERFERin reagent (Polyplus) at a final concentration of 50 nM. The full-length PTBP1-CDS was cloned from our lab (Zhu et al., 2019). All plasmids were purified using an Endo-Free Plasmid Maxi Kit (QIAGEN) and transfected into U87MG cells using FuGENE6 (Promega).

RT-PCR and PCR

Total RNA was purified using an RNeasy Mini Kit (QIAGEN) according to the manufacturer's protocol. Two micrograms of total RNA was used as a template for cDNA synthesis with Trans-Script First-Strand cDNA Synthesis Super-Mix (AT301-02, Trans-Gen Biotech). The reaction mixture was incubated at 42°C for 30 min and then inactivated at 85°C for 5 s. Full-length HOTAIRM1 and the DNA fragments used for RNA probes were amplified with Phanta Max Super-Fidelity DNA Polymerase (P505-d1, Vazyme). The primers are listed in Table S6.

Real-time PCR

cDNA was synthesized with HiScript II Q RT Super-Mix for qPCR (+gDNA wiper) (R223-01, Vazyme). Genomic DNA removal was performed at 42°C for 2 min. The reverse transcription reaction was performed under the following conditions: 50°C for 15 min and then 85°C for 5 s. Real-time PCR was performed with

SYBR Premix EX Taq (RR420A, TaKaRa) using a CFX96 Touch system (BioRad, USA). The Ct values of the target genes were normalized to those of the β -actin or GAPDH gene. The $\Delta\Delta$ Ct method was used to determine the relative expression levels of the target genes. All samples were run in triplicate in each experiment. The sequences of the primers are listed in Table S5.

Western blot analysis

Whole cells or tissues were collected and homogenized with TNTE lysis buffer containing protease and phosphatase inhibitors. After incubation for 40 min on ice, the homogenate was centrifuged at 12,000 rpm for 30 min at 4°C. The supernatants were denatured at 98°C for 10 min with 6× loading buffer to generate the samples for western blotting. Proteins in the samples were separated on a 10% SDS-PAGE gel and transferred onto BioTrace nitrocellulose membranes (66,485, Pall Corporation). After blocking for 0.5 h in 5% nonfat milk diluted with Tris-buffered saline containing 0.1% Tween 20 (9005-64-5, VWR Chemicals), the membranes were incubated first with various primary antibodies and then with horseradish peroxidase-conjugated secondary antibodies (ZB-2301/ZB-2305, ZSGB-Bio). Immunoreactivity was visualized with a SuperSignal West Pico PLUS kit (34,580, Thermo Scientific).

Cell proliferation assays

An MTS assay (Promega, USA) was used to evaluate the short-term proliferation ability of glioma cells. Cells were seeded at a density of 3000 cells per well in 100 μ L of medium per well in 96-well plates. Twenty microliters of MTS (2 mg/mL DPBS)/PMS (0.92 mg/mL DPBS) detection solution was added to each well and incubated for 2 h. The absorbance was measured at a test wavelength of 490 nm and a reference wavelength of 630 nm to calculate the sample signals. Data are presented as the mean \pm SD of three independent MTS assays. A colony formation assay was used to evaluate the long-term proliferation ability of glioma cells. Glioma cells with lentivirus-mediated stable knockdown of HOTAIRM1 were plated in 6-well plates at 500 cells per well. Ten to 14 days later, the cell colonies were stained with crystal violet and photographed.

Cell migration and invasion assays

For the Transwell migration assay, U87MG, T98G and A172 cells were used, and 5×10^4 cells were seeded on 8 μ m pore size Transwell filters (Corning). For the invasion assays, 1×10^5 U87MG and A172 cells were seeded in the upper chamber of each compartment on an insert coated with 150 μ g Matrigel (BD BioCoat). The cells were resuspended in serum-free medium and induced to migrate toward medium containing 20% FBS for 24 h (migration assay) or 48 h (invasion assay) in a CO₂ incubator. Nonmigrated and noninvaded cells were removed with a cotton swab. The remaining cells were fixed and stained with dye solution containing 20% methanol and 0.1% crystal violet. The cells that had migrated or invaded were imaged using an IX71 inverted microscope (Olympus Corp.). Ten random fields were chosen, and the cell numbers were averaged. The graphs indicate the average number of migrated or invaded cells per field of glioma cells. The data show the mean \pm SD of three independent experiments.

Mitochondrial and cytosolic fractionation

We used a Cell Mitochondria Isolation Kit (C3601, Beyotime, China) to isolate the mitochondria and cytoplasmic proteins of cultured cells. First, 2 mL of mitochondrial separation reagent supplemented with phenylmethylsulfonyl fluoride (PMSF) was added to 4×10^7 precipitated A172 cells digested with trypsin-EDTA solution and placed in an ice bath for 15 min after resuspension. The cell suspension was transferred to a glass homogenizer and homogenized for approximately 20 cycles. After centrifugation at $1000 \times g$ and 4°C for 10 min, the supernatant was carefully transferred to another centrifuge tube, and then centrifuged at $3500 \times g$ at 4°C for 10 min. The resulting precipitate was the isolated mitochondrial fraction; mitochondrial proteins were isolated by adding 200 μ L of mitochondrial lysis buffer supplemented with PMSF, and mitochondrial RNA was extracted with TRIzol reagent according to the manufacturer's instructions (15,596,018, Invitrogen). The resulting supernatant was collected and centrifuged at $12,000 \times g$ and 4°C for 10 min, and the supernatant was the cytoplasmic fraction with all mitochondria removed.

RNA fluorescence *in situ* hybridization

To detect the subcellular localization of HOTAIRM1, RNA FISH was carried out with *in vitro* transcribed digoxigenin-labeled antisense probes for HOTAIRM1-1 and HOTAIRM1-2 (Roche Applied Science). Briefly, T98G cells were fixed with DEPC-4% PFA for 10 min. Then, the cells were incubated with denatured

Dig-labeled FISH probes in hybridization buffer (50% formamide in 0.2× SSC) at 65°C overnight. After hybridization, an anti-POD antibody and TSA were sequentially added to visualize the signals with TSA Plus fluorescence systems (PerkinElmer). Cells were observed with a confocal laser microscope (FV1000; Olympus). Nuclei were counterstained with DAPI.

Seahorse assays

The oxygen-consumption rate (OCR) was measured in U87MG, T98G and A172 glioma cells using a Seahorse XF Extracellular Flux Analyzer (Seahorse Bioscience). Twenty-four-well plates (Seahorse Bioscience) were coated with 50 μL of poly-D-lysine (10 μg/mL) for 2 h and were then coated with laminin (10 μg/mL) overnight. The next day, the wells were washed twice with PBS, and 2–5 × 10⁵ cells were plated in each well. Three metabolic inhibitors were injected sequentially at specific time points: oligomycin (1 μM), followed by FCCP (0.75 μM), followed by a combination of rotenone and antimycin A (0.5 μM). The basal OCR was measured using the Seahorse XF24 plate reader.

In vivo mouse models

For the intracranial xenograft model, shNT- or shHOTAIRM1-U87MG cells (5 × 10⁵ cells/mouse) were collected and resuspended in 5 μL of PBS and injected into the frontal cortex (1 mm rostral to the bregma, 1.5 mm lateral to the midline and 3.5 mm deep) of mice (4 mice per group) using a Hamilton microsyringe. Tumor bearing mice were killed 30 days after inoculation, and the brains were excised for hematoxylin and eosin (H&E) staining. For the subcutaneous xenograft model, shNT- or shHOTAIRM1-U87MG or A172 cells (5 × 10⁶ cells/mouse) resuspended in 200 μL of PBS were implanted subcutaneously into the right forelegs of nude mice (10 mice per group). The tumor volume in each group was determined beginning on the first day when visible tumors were found. Tumor growth was monitored by measuring the tumor lengths and widths, on the 1st, 4th, 6th, 8th, 11th, 13th, 15th, 18th, 20th, 22nd and 25th days and calculating the volume with the following formula: $V = L \times W^2 \times \pi/6$ (V, volume; L, length; W, width). The survival rates were recorded and analyzed after all control mice died.

Dual luciferase promoter reporter assay

Three human *SHMT2* promoter regions (−1145~+208, −1028~+205 in the *SHMT2* gene encoding transcript variant 1, and −189~+61 in the *SHMT2* gene encoding transcript variant 7) were amplified by PCR using human genomic DNA as the template, and were then cloned into pGL3-Basic vectors (Promega) containing a firefly luciferase reporter gene to obtain the pGL3-SHMT2 constructs (P1, P2 and P3). First, siHOTAIRM1-1 (si-1), siHOTAIRM1-2 (si-4), siHOTAIRM1-1/2 (si-5) and the control siRNA (NC) were transfected into U87MG, T98G and A172 cells in 24-well plates using INTERFERin reagent (Polyplus) at a final concentration of 50 nM. After 24 h, the three cell lines were cotransfected with 0.2 μg of pGL3-SHMT2 along with 50 ng of pRL-TK (Promega) using FuGENE 6 reagent (Promega). After 48 h, the luciferase activity was measured with a dual-luciferase assay system according to the manufacturer's instructions (Promega).

Enhanced CLIP-seq

eCLIP experiments were performed according to a published protocol (Van Nostrand et al., 2016). A total of 2 × 10⁷ A172 cells incubated for 3 h with 500 μM 4-thiouridine (4SU; T4509, Sigma) were crosslinked with 2 × 400 mJ/cm² doses of 365 nm UV light and snap frozen. The cells were then lysed with 1 mL of CLIP lysis buffer (50 mM Tris-HCl (pH 7.4), 100 mM NaCl, 1% NP-40, 0.1% SDS, and 0.5% sodium deoxycholate) with the temporary addition of 1 mM DTT (P2325, Gibco), 5.5 μL of 200 × protease inhibitor cocktail III (539, 134-1SET, Calbiochem/Merck) and 11 μL of RNase inhibitor (N2515, Promega) and were then treated with RNase I (AM2295, Invitrogen by Thermo Fisher Scientific) to fragment the RNA. An anti-PTBP1 or anti-IGF2BP2 antibody (RN011P/RN008P, MBL Beijing Biotech Co., Ltd) was then pre-conjugated to Protein A Dynabeads (10002D, Invitrogen by Thermo Fisher Scientific), added to the lysate, and incubated overnight at 4°C. Before immunoprecipitation, 2% of the sample was taken as the paired input sample. The remaining samples were ligated to RNA adapters, washed and separated magnetically. After SDS-PAGE and membrane transfer, we excised the gel slices from ~55 kDa to ~130 kDa (PTBP1 eCLIP) and from ~65 kDa to ~140 kDa (IGF2BP2 eCLIP), and then treated them with proteinase K (P8107S, New England Biolabs) to release the RNA. Furthermore, reverse transcription, DNA adapter ligation, and PCR amplification were performed to construct the DNA libraries. The DNA libraries were purified on 3% low melting temperature agarose gels (50,070, Lonza), gel slices from 175 to 350 bp were excised, and DNA was eluted with a Qiagen MinElute gel extraction kit. All eCLIP experiments were performed twice. Finally, high-throughput

sequencing was conducted on the Illumina HiSeq platform. CLIPper software was used for peak analysis. The accession number for the eCLIP-seq data reported in this paper is GEO: GSE192792.

Ribonucleoprotein immunoprecipitation

Ribonucleoprotein immunoprecipitation (RIP) was performed in native U87MG and A172 cells and cells with stable lentivirus-mediated knockdown (shNT-A172 and shHOTAIRM1-A172). First, 15 μg of an anti-PTBP1 (RN011P, MBL), anti-IGF2BP1 (RN007P, MBL), anti-IGF2BP2 (RN008P, MBL) or anti-IGF2BP3 (RN009P, MBL) antibody and ~ 40 μL of Protein A agarose beads (11,719,408,001, Roche Diagnostics) were incubated with rotation overnight at 4°C (normal rabbit IgG was used as the negative control). Second, 2×10^7 cells per sample were collected and incubated with 500 μL of lysis buffer (containing 1.5 mM DTT, appropriate concentrations of protease inhibitors and 200 U/mL RNase inhibitor) for 15 min on ice. The centrifuged supernatant was transferred to antibody-bound Protein A agarose beads and incubated with rotation for 3 h at 4°C. Finally, the antibody-bound Protein A agarose bead-ribonucleoprotein complexes were washed, and RNA was isolated from these complexes according to the RIP-Assay Kit instructions (RN1001, MBL). Related enrichment of mRNAs was detected by real-time PCR.

Biotin pulldown

Fragments of HOTAIRM1 or SHMT2 RNA were inserted into the pGEM-3zf vector containing a T7 promoter. The primers are listed in Table S6. The biotin-labeled sense RNA probes were synthesized *in vitro* using T7 RNA polymerase (2540B, Takara Bio) and Biotin RNA Labeling Mix (11,685,597,910, Roche). The antisense GFP RNA probe was used as the negative control. Samples containing unlabeled RNA probes or no RNA probes were also used as experimental controls. Cytoplasmic and nuclear extracts were isolated from U87MG, T98G and A172 cells using NE-PER Extraction Reagent (78,835, Thermo Fisher Scientific). RNA affinity capture was subsequently conducted with streptavidin Sepharose beads (17-5113-01, GE). Briefly, a reaction mixture containing 200 μL of cell extract and ~ 3 μg of biotin-labeled or unlabeled RNA probe was prepared. The mixture was supplemented with 800 μL of RNA binding buffer containing 10 mM HEPES (pH 7.5) (15,630-080, Gibco), 50 mM KCl (AM9640G, Invitrogen by Thermo Fisher Scientific), 0.5% NP40 (NP40S, Sigma), 1.5 mM MgCl_2 (AM9530G, Invitrogen by Thermo Fisher Scientific), 2 mM DTT, 1 mM EDTA (AM9260G, Invitrogen by Thermo Fisher Scientific), 100 U/mL RNase inhibitor, protease inhibitors, 400 μM ribonucleoside vanadyl complex (S1402S, New England Biolabs) and 100 $\mu\text{g}/\text{mL}$ tRNA from *Escherichia coli* (R1753, Sigma), was incubated for 30 min at 30°C and then added to 200 μL of streptavidin Sepharose beads for 60 min at room temperature to allow binding. The beads were washed four times with RNA binding buffer. Proteins on the beads were eluted from the bound RNAs by incubation at 98°C for 10 min and analyzed by western blotting.

Protein immunoprecipitation assay

For the protein immunoprecipitation assay, equal amounts (~ 1000 μg) of cell lysates were incubated with a 1/100 (w/w) dilution of the anti-PTBP1, anti-IGF2BP1, anti-IGF2BP2 or anti-IGF2BP3 antibody (MBL) or with normal rabbit IgG as the negative control overnight at 4°C. Aliquots of the extracts from shHOTAIRM1-treated cells and shNT-treated cells were exposed to RNase. Subsequently, the lysates were incubated with Protein A/G Plus Agarose (Pierce) in spin columns and mixed with end-over-end rotation for 1 h. The resin was washed four times, and immunocomplexes were eluted according to the instructions of the Pierce Classic IP Kit (26,146, Thermo Fisher Scientific). The protein samples were analyzed by Western blotting.

RNA stability

RNA stability was analyzed using 5'-bromouridine (BrU) immunoprecipitation chase (BRIC) Kit (RN1007/RN1008, Medical & Biological Laboratories Co., Ltd., Nagoya, Japan). In brief, for the BRIC assay, after siRNA transfection or lentiviral transduction, cells were incubated at 37°C in medium containing 150 μM BrU for 24 h in a humidified incubator with 5% CO_2 . After the BrU-containing medium was replaced with BrU-free medium, cells were harvested at 0, 2, 4, 6, and 8 h. Total RNA was denatured by heating at 80°C for 2 min and then added to anti-BrdU mAb-conjugated protein G magnetic beads. The mixture was incubated at 4°C for 3 h with rotation. The beads were washed, and RNA was isolated according to the manufacturer's instructions.

Methylated RNA immunoprecipitation

For m⁶A RIP, we used an anti-m⁶A antibody (clone 17-3-four to one, MABE1006, Millipore Sigma) and normal mouse IgG (CS200621, Millipore Sigma) as one negative control to immunoprecipitate m⁶A-modified *SHMT2*. Total RNA was isolated from five 10-cm dishes using an RNeasy Mini Kit (QIAGEN). For each precipitation reaction, we used approximately 300 µg of total RNA divided into 1 µg/µL aliquots, for a total of 18 µL per tube. The fragmentation process was conducted at 94°C for 1 min to produce RNA fragments with a size distribution centered on ~100 nt, and 300 µL of the fragmented RNA was purified. Ten percent of the total RNA was removed as “RNA input”. Then, 10 µg of the anti-m⁶A antibody or normal mouse IgG was added to 100 µL of 1×IP buffer per 25 µL of protein A/G magnetic beads (CS203152, Millipore Sigma) and incubated with rotation for 30 min at room temperature. The MeRIP reaction mixture (1000 µL) was prepared, added to each tube containing bead-antibody conjugates and incubated with rotation for 2 h at 4°C. The beads were washed 3 times, and 100 µL of elution buffer containing 20 mM N⁶-methyladenosine (CS220007) was added to completely resuspend the beads before incubation with continuous shaking for 1 h at 4°C. Finally, m⁶A-bound RNA was extracted with RNA Clean & Concentrator-5 (R1016, Zymo Research), and the levels of *SHMT2* RNA and the control RNA *EEF1A1* were measured by qPCR. For the positive and negative controls, we detected the known m⁶A-modified and non-m⁶A modified fragments of *EEF1A1* mRNA (Jin et al., 2018). We used the $\Delta\Delta C_t$ method to analyze the data.

LncRNA microarray analysis

Total RNA from ~10⁶ shNT-U87MG, shHOTAIRM1-U87MG, shNT-T98G, shHOTAIRM1-T98G, shNT-A172 and shHOTAIRM1-A172 cells was extracted using TRIzol reagent (Invitrogen, USA). RNA integrity was assessed on an Agilent Bioanalyzer 2100 instrument (Agilent Technologies, Santa Clara, CA, USA). The qualified total RNA was further purified by using a NucleoSpin RNA Clean-Up Kit (740.948.250, Macherey-Nagel). cRNA was synthesized and then cDNA was then reverse transcribed and purified with NucleoSpin Extract II (740.609.250, Macherey-Nagel). The labeled cDNA was used for hybridization on a Genechip Agilent Human lncRNA 4 × 180 K array (Agilent Technologies). The slides were scanned in an Agilent Microarray Scanner (Agilent Technologies) with the default settings at CapitalBio Corporation. The quantile algorithm (Gene Spring Software 11.0, Agilent Technologies) was used for normalization of raw data. The HOTAIRM1 knockdown microarray data have been deposited in the GEO repository under accession number GEO: GSE192627.

Protein silver staining and mass spectrometry

Silver staining was performed to compare the proteins associated with biotin-labeled HOTAIRM1-1 or HOTAIRM1-2 with those associated with unlabeled RNA probes and antisense probes. The protein samples from the biotin pulldown assay were separated using 10% SDS-PAGE, and the gel was then incubated with the stationary phase (40% methanol and 10% acetic acid) for 30 min. After washing with washing buffer five times, the gel was further incubated with sensitization buffer (30% ethanol, 0.068 g/mL sodium acetate, and 0.0325 g/mL Na₂S₂O₃) two times for 15 min each. The gel was later incubated first with silver staining buffer for 30 min in the dark and then with color reagent (4 g of Na₂CO₃, 80 µL of formaldehyde, and 200 mL of H₂O) for 6 min. The 30 stained protein bands visible on the gel after silver staining were excised, digested, and analyzed by liquid chromatography-tandem mass spectrometry (LC-MS/MS) in the National Center of Biomedical Analysis. Sequence analysis was performed with MASCOT (version 2.2, Matrix Sciences, Boston, MA, USA) using the nonredundant protein database from Mascot’s website (<http://www.matrixscience.com/>). The bound proteins were screened according to ion scores and the exponentially modified Protein Abundance Index (emPAI).

Metabonomic analysis

A total of 1 × 10⁷ shNT-, shSHMT2-, and shHOTAIRM1-A172 cells per sample were cultured in complete medium or nonessential amino acid-free medium for 48 h. Cell precipitates were collected and quickly frozen in liquid nitrogen. All samples were analyzed in triplicate. High-throughput target quantification of amino acids and detection of tetrahydrofolate and 5,10-methylenetetrahydrofolate were completed at Shanghai Biotree Biotech Corporation. The UHPLC separation was carried out using an Agilent 1290 Infinity II Series UHPLC System (Agilent Technologies) equipped with a Waters ACQUITY UPLC BEH Amide Column (100 × 2.1 mm, 1.7 µm). Agilent MassHunter Work Station Software (B.08.00, Agilent Technologies) was employed for MRM data acquisition and processing. Calibration solutions were subjected to

UPLC-MRM-MS/MS analysis. The metabolite concentration in nmol/g equals the final amount of the metabolite in the sample divided by the protein concentration of the sample.

QUANTIFICATION AND STATISTICAL ANALYSIS

Cell culture experiments were performed at least three times and in at least triplicate for each replicate experiment. Data are presented as the means \pm standard deviations. For experiments with 2 comparisons, 2-tailed Student's *t* test was used for statistical analysis. For comparisons among more than two conditions, one-way ANOVA with the unpaired *t* test, Dunnett *t* or Tukey's test for multiple comparisons was used. *p* values <0.05 were considered statistically significant and are marked on the graphs by asterisks (**p* < 0.05 , ***p* < 0.01 , ****p* < 0.001). All analyses were performed using Prism 5.0 software. The Kaplan-Meier plotter or logrank test was used to evaluate patient and mouse overall survival. Mice were randomly assigned to groups. Correlation analyses were performed by calculating the Pearson or Spearman correlation coefficient. No samples or animals were excluded from the analyses.